REVIEWS

Journal of Semiconductors
(2020) 41, 091708
doi: 10.1088/1674-4926/41/9/091708

Perylene diimide self-assembly: From electronic structural modulation to photocatalytic applications

Weiqin Wei, Shuxin Ouyang†, and Tierui Zhang

College of Chemistry, Central China Normal University, Wuhan 430079, China

Abstract: As an emerging organic semiconductor, perylene diimide (PDI) self-assembly has attracted tremendous attention in the aspects of solar cells, sensors, fluorescence probes and n-transistors, etc. In term of photocatalysis, various photocatalysts based on PDI self-assembly exhibit some unique properties, such as intrinsic Π-Π stacking structure, fast internal charge transfer, band-like electronic structure, flexible structural modifiability, well-defined morphological adjustability and excellent light absorption. This paper mainly presents recent progress on PDI self-assembly regarding how to regulate the electronic structure of PDI self-assembly. In addition, the photocatalytic applications of PDI self-assembly and its complexes were reviewed, such as environmental remedy, energy productions, organic synthesis and photodynamic/photothermal therapy, further highlighting related photocatalytic mechanisms. Finally, the review contents and some perspectives on photocatalytic research of PDI self-assembly were summarized, and some key scientific problems were put forward to direct related photocatalytic research in future.

Key words: perylene diimide; self-assembly; photocatalysis; Π-Π stacking; electron transfer

Citation: W Q Wei, S X O yang, and T R Zhang, Perylene diimide self-assembly: From electronic structural modulation to photocatalytic applications[J]. *J. Semicond.*, 2020, 41(9), 091708. http://doi.org/10.1088/1674-4926/41/9/091708

1. Introduction

The sharply increasing threat posed by energy shortage and environmental pollution exerts a substantial impact on modern economic development and human living environment[1, 2]. For example, every year there is average net CO_2 uptake of 2.1 gigatons of carbon dissociated into the ocean, causing serious oceanic acidification[3]; excessive atmospheric CO_2 and SO_2 emitted from fossil fuel combustion leading to global climate variability (e.g. global warming and regional climate anomaly)[4, 5]. Therefore, it is considerably urgent to exploit an earth-abundant, secure and eco-friendly alternative to conventional fuel resources. Semiconductor-based photocatalysis is becoming a promising strategy to fit this requirement well. The technology only needs the solar energy that is renewable, secure and "green", and the photocatalysts that can convert absorbed light into other kinds of chemical energies[6, 7]. It has been intensively employed in the elimination of environmental pollutants[8–10], water splitting into H_2/O_2[11, 12], H_2O_2 production[13], CO_2 reduction into C_1 feedstock/hydrocarbons[14, 15], selective organic synthesis[16, 17], disinfection of bacteria[18] and treatment of tumors[19], etc.

Traditionally, inorganic semiconductors have been widely employed in the field of photocatalysis, e.g. TiO_2[20], CdS[21, 22], ZnO[23, 24], SnO_2[25, 26], Bi_2WO_4[27, 28], Bi_2VO_4[25, 29] and $InTaO_4$[30]. Two key problems is weak visible-light absorption and the high combination of photoinduced carriers in inorganic semiconductors, largely limiting the practical application and development of photocatalysts[6, 7]. Furthermore, albeit with the delivery of visible-light absorption for some inorganic semiconductors, some of them would suffer from irreversible photocorrosion and decayed photocatalytic performance[31]. Importantly, how to effectively regulate the electronic structures of inorganic semiconductors still remains highly challenging. Therefore, it is necessary to develop a material that can readily adjust its electronic structure to obtain efficient photocatalytic performance.

Recently, emerging organic semiconductors have aroused substantial attention owing to flexible structural modification, changeable electronic energy bands, tunable morphologies, superior light absorption, excellent chemical stability and versatile functions[32, 33]. As a typical representative, polymeric carbon nitride (abbreviated as CN) is a traditional two-dimensional sheet material with the most stable allotrope of C_3N_4[34]. The past decade has witnessed an explosion of literature involving CNs in numerous research fields, including biomedical applications[35], electrochemiluminescence analysis[36], spintronic devices[37], energy conversion/storage[38], chemical sensors[39], photo(electro)catalysis[40, 41], etc., especially in photocatalysis. Since 2006, Wang *et al.* unraveled its surprising visible-light photocatalytic performance for water splitting, because CNs own a narrower band gap of ca. 2.7 eV, with adequate conduction band (CB) and valence band (VB) levels for water splitting[42]. Scientists gradually attach importance to organic photocatalysts by predominant virtue of tunable energy band potentials via simple chemical modification to molecule structures. These organic photocatalysts not only include isolated molecular photocatalysts with metal ion coordination (Mn[43], Cr[44], Ni[45], Pt[46], Co[47], Ir[48], Ru[49, 50], Rh[49], etc.) or metal-free molecular photocatalysts[51], but also include a variety of metal organic frameworks (MOF)[52–54], covalent organic frameworks (COF)[55, 56], conducting conjugated polymers (e.g. poly(diphenylbuta-

Correspondence to: S X O yang, oysx@mail.ccnu.edu.cn
Received 31 MAY 2020; Revised 12 JUNE 2020.

diyne)[32], poly(3-hexylthiophene)[57, 58], poly(2-methoxy-5-)2-ethylhexyloxy-1,4-phenylene vinylene[57], poly(p-phenylene)[59], polypyrrole[60], polyisoprene[60] and poly(3,4-ethylenedioxythiophene)[61]), a porous conjugated polymer coordinated with metal ions[62] and supramolecular self-assemblies that are constituted of molecular building blocks under non-covalent interactions[63–65].

Textile dyes have a long history of ca. 150 years as the first products in most of the largest chemical companies founded at that time[66]. Mostly, the colorants are utilized in the form of monomeric dyes. As exceptions, some counterparts form bulk materials via non-covalent interactions and possess crystalline features, which are usually renamed as pigments[67]. These pigments present particular optical/electronica/chemical properties different from monomeric dyes, owing to various self-assembled structures[66, 68]. The dye–dye interactions can strongly affect the structures, morphologies and coloristic properties of bulk materials, for instance, forming organic semiconductors. This type of organic semiconductor is usually composed of many semi-planar molecules with large conjugated Π-bond and rigid structure, such as porphyrin, pentacene, rubrene, hexamethylenetetratellurafulvalene, bis(1,2,5-thiadiazolo)-p-quinobis(1,3-dithiole), violanthrone B, perylene monoimide, 2-cyano-10-methyl-5-phenazyl, 1,8-naphthalimide, 7,7,8,8-tetracyanoquinodimethane, perylene-3,4,9,10-tetracarboxylic acid diimide[69]. Among them, perylene diimide derivatives act as one common type of these pigments (abbreviated as PI, PDI, PBI or PTCDI from perylene-3,4,9,10-tetracarboxylic acid diimide)[66, 68]. The molecule unit is consisted of PDI core and side chains. Interestingly, due to the great Π-extended structure of the perylene ring of individual molecule, the intrinsic Π–Π stacking interaction of each building block occurs along the one-dimensional direction if suitable solvents are given[70]. Together with hydrogen bonds or other noncovalent interactions, it eventually affords a supramolecular self-assembly with a highly ordered structure. Chemical modification to perylene ring and side chains can easily tune self-assembled modes and supramolecular constructions[66, 68]. Consequently, a variety of morphologies, e.g. hollow nanosphere[71], rectangular plate[71], spheroid[72], spiral[73], wire[8], rod[74] and fiber[72, 75], can be constructed in specific dispersion media. The process of forming supramolecular architectures demonstrates in essential a dynamic equilibrium between gel and sol; therefore, environmental factors (such as solvent, temperature, concentration) are of utmost importance towards a pathway-controlled self-assembly of well-organized structures[73, 76]. As a result, modulating microscopic molecular stacking arrangements between PDI molecules is a sticky challenge because the balance state is strongly sensitive to environmental conditions. Different Π–Π stacking modes could result in distinctly different electron-transfer pathways and thus change photocatalytic performances[8, 10]. The aggregation endows it a broader light-absorption range, even extending to the near-infrared region via changing the molecular stacking columns (such as J- and H-type aggregation) as has been evidenced by experiments and DFT calculations[10, 77]. Importantly, electron transfer along the Π–Π stacking direction is a salient characteristic in photocatalysis[78–80] which can effectively prevent the combination of photogenerated electrons and holes. Furthermore, the supramolecular can form a band-like electronic structure with CB and VB levels, and enable photoinduced charge delocalization along the Π–Π stacking direction[64]. Hence, as a metal-free photocatalyst, PDI self-assembly possesses its own electronic structure similar with common inorganic semiconductors, delivering three basic photocatalytic processes including light harvesting, charge separation and charge transportation, and importantly exhibits some impressive performances largely attributable to the Π–Π stacking structure and consequential electron transfer along the Π–Π stacking direction. Given these properties, PDI self-assembly can effectively utilize the wider solar-light spectrum and inhibit combination of photogenerated electrons and holes; therefore, PDI self-assembly-based photocatalysts and its composites have been employed in photocatalytic degradation of organic contaminants[8–10, 19, 74, 81–86], photocatalytic water splitting[64, 74, 83, 85, 87–88], disease therapy[19, 89] and photocatalytic organic synthesis[16, 90]. Although some exceptional reviews on PDI self-assembly have been published in the fields of supramolecular, optoelectronics, synthesis and biology[66, 68, 91–94], to the best of our knowledge, there are currently no comprehensive reviews on photocatalysis of PDI self-assembly. The modulation of electronic structures of photocatalysts plays a dominant role in improving its photocatalytic performance. Therefore, it is necessary to systematize the relationship between the structure, electronic structure and photocatalytic performance of PDI self-assembly to provide a reference for future photocatalytic research on self-assembly analogues.

Herein, we present the overview from the electronic structural modulation to photocatalytic applications of PDI self-assembly-based photocatalysts. Firstly, the basic characteristics of PDI molecules and PDI self-assembly are introduced. Next, the possible electronic modulation approaches are discussed, including modifying perylene areas, tuning Π–Π stacking via side-chain substituents, constructing PDI self-assembly-based composites and the role of PDI anion/dianion radicals. Subsequently, some practical applications are exemplified to highlight the significance of the organic self-assembled materials, including photocatalytic degradation of pollutants, water splitting into H_2/O_2, organic synthesis and disease therapy, with high efficiency of solar-light utilization stemming from particular Π–Π stacking structures. Finally, the outlooks and perspectives on further development of PDI self-assembly-based photocatalysts are envisioned.

2. Basic characteristics of PDI molecules

Individual PDI molecule derivatives consist of two primary motifs-PDI skeleton and side chains. The PDI skeleton can be considered as being composed of a nonpolar perylene ring and two polar cyclic amides. Π-conjugated perylene fragment endows PDI molecules a strong self-assembled propensity and electron delocalization possibility along the Π–Π stacking direction via intermolecular orbital overlapping. Viewing from the bond lengths of PDI molecules (Figs. 1(a) and 1(b)), the two Csp^2–Csp^2 bonds that connect two naphthalene half units appear to be longer than the other Csp^2–Csp^2 bonds and would undoubtedly generate steric strain in the coplanar perylene core. Consequently, two naphthalene half units in the perylene ring are twisted with a

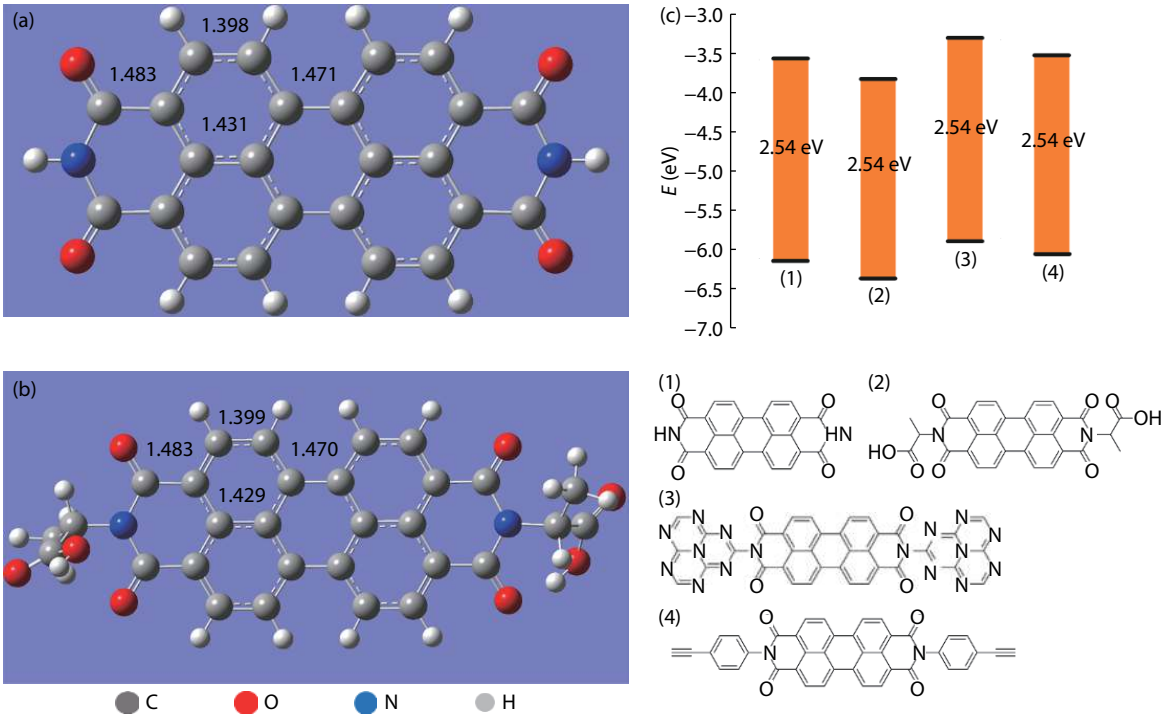

Fig. 1. (Color online) Bond lengths of PDI molecules (a) without side chains and (b) with side chains obtained via DFT calculations. (c) Frontier orbital energy levels of PDI molecules (1), (2), (3) and (4). (Method and basic set: B3LYP 6-31+G*).

torsional angle[68], thus slightly damaging the planar Π-conjugated structure of the perylene ring. In particular, PDI molecules with perylene rings substituted by some sterically hindered functional groups display more significant torsional angles[95, 96]. The distortion conformation could increase PDI solubility in organic solvents and make it possible to react with some reagents to link desired functional groups. Nonetheless, plenty of PDI derivatives are not easily dissolved with a large required amount in most of the organic solvents, even universal solvents N,N-dimethylformamide (DMF) and dimethyl sulfoxide (DMSO), hence it still remains notoriously challenging to functionalize and purify massive PDI products in common solvents. Another equivalently important unit is side chains at both ends of PDI molecules. Via simple reflux reaction using perylene tetracarboxylic acid disanhydride (PTCAD) and a wide series of primary amine molecules as reacting substrates, PDI molecules with various side chains can be easily synthesized[92]. Usually, the electron density at the nodes of the highest occupied molecular orbital (HOMO) and lowest unoccupied molecular orbital (LUMO) of PDI molecules nearly approaches to zero[97], meaning that side-chain motifs do not readily engage in Π-electron conjugation with a perylene ring and fail to significantly affect the overall electronic structures of PDI molecules[72]. Hence, the corresponding redox potentials and optical properties remain almost invariant, especially molecular energy level gaps (Fig. 1(c))[92]. But side-chain substituents can remarkably enhance their solubility, for instance, carboxyl groups connected at side chains can enable it to dissolve in alkaline solutions[16]. Besides, the formation of self-assembled supramolecular requires the participation of side chains which offer hydrogen bonds and side-to-side chain interactions to stabilize the lateral growth of PDI self-assembly albeit the main driven force from Π–Π stacking along the longitudinal direction.

3. Aggregation characteristics in thermodynamics

The packing characters have been deeply discussed in the reviews of Würthner's group[66, 68]. Owing to Π-conjugated structures of PDI molecules, Π–Π stacking behaviors between PDI molecules are presented with a parallel arrangement distance between 3.34 and 3.55 Å, analogue to the distance between graphite layers (3.35 Å) (Fig. 2(a))[100, 101]. The d-spacing distances of 3.34 and 3.55 Å are attributed to cofacial Π–Π stacking distance (H-type) and twisted arrangement (J-type) in parent PDI, respectively[8]. The stacking distance is greatly influenced by steric hindrance of imide substituents, namely side-chain-dependent interaction[74]. In general, coplanar Π–Π stacking results in the maximization of PDI molecular orbital overlap. But in fact, due to the influence from its own molecule structure and external environment, the degree of PDI molecular orbital overlap usually corresponds to partially overlapping Π–Π stacking, such as J-type aggregation. The rotation between neighboring molecules in columns is mainly favored through intermolecular dipole-dipole interactions between C=O of the imide moieties[102]. Zang and coworkers found that polarized fluorescence spectra can be used to reveal PDI tilted stacking conformation of PDI self-assembly along the belt direction[103]. H-type aggregate with high-energy signatures in absorption spectra is attributable to coulombic coupling, while the J-like aggregate with low-energy signatures is caused by short-range charge-transfer-mediated coupling[104]. Moreover, transverse offset of perylene rings with respect to each other determines the bay-to-bay contact area and interaction degree between molecular orbitals. The stacking distance, longitudinal and transverse offset between neighboring PDI molecules altogether influence optical properties of PDI self-assemblies, including bathochromic shift, absorption band broadening and seemingly color presence, etc. In general, PDI self-assembly

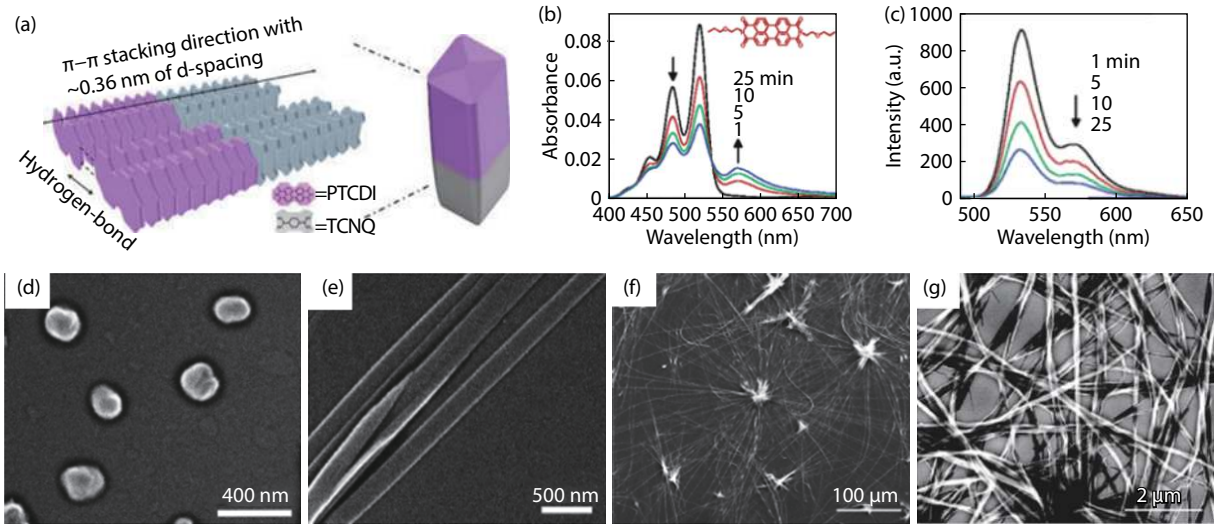

Fig. 2. (Color online) (a) Model diagram of the PDI Π–Π stacking-assembled structure with permission from Ref. [86]. Crystal formation of propoxyethyl-PDI in methanol: (b) absorption, fluorescence and (c) spectra recorded at different time intervals following the injection of a minimal volume of chloroform solution with permission from Ref. [75]. (d) A higher magnification image showing discrete particles in approximately spherical shape with permission from Ref. [72]. (e) A higher-magnification image showing discrete, straight nanobelts, on which another belt is piled in a twisted conformation with one edge faced up with permission from Ref. [72]. (f) A large-area SEM image showing the growth of long nanobelts from the central seeding particulate aggregates with permission from Ref. [98]. (g) SEM image of pristine nanofibers deposited on the silica with permission from Ref. [99].

presents two major absorption bands (ca. 490 and 550 nm) in the UV–visible absorption spectrum. The former is attributable to electronic transition of individual PDI molecules while the latter originates from Π–Π stacking interaction inside PDI self-assembly[75, 98]. In specific solvents, isolated PDI molecules tend to aggregate spontaneously forming ordered nanocrystal through Π–Π stacking and side-to-side chain interactions. Balakrishnan *et al.* detected crystal formation process of propoxyethyl-PDI in methanol via UV–visible absorption spectroscopy (Fig. 2(b)). With an increase of self-assembling time, the absorption bands (0–0, 0–1, 0–2, and 0–3 at 520, 485, 455, and 426 nm, respectively) of PDI molecules decreased while that at 550 nm increased, suggesting crystal formation[75]. The isobestic point at 536 nm showed up, indicating self-assembling process from the isolated PDI molecules to the PDI self-assembly. In addition, due to the charge transfer along the Π–Π stacking direction, the photogenerated electrons and holes in PDI self-assembly are spatially separated, directly causing a decrease in fluorescence emission compared to PDI molecules (known as aggregation-induced quenching behavior). Fig. 2(c) demonstrated that Π–Π stacking resulted in a decrease of fluorescence emission due to forbidden transition. In the highly crystalline Π–Π stacking aggregates, due to the restricted movement of molecules, the non-radiation decay rate of the excited states can compete with the radiation decay rate, resulting in the more obvious fluorescence decrease[105]. Additionally, Balakrishnan *et al.* found that the morphologies of PDI self-assembly can be effectively controlled via the hindered effect of side-chain substituents (Figs. 2(d) and 2(e))[72]. In their report, two different imide substituents were introduced into the PDI molecules, respectively. Obviously, the PDI with smaller steric hindrance formed a one-dimensional structure. By contrast, due to larger steric hindrance to Π–Π stacking between PDI chromophores along the longitudinal direction, the zero-dimensional self-assembly was thus constructed. Only if Π–Π stacking interaction between PDI molecules is strong enough, the Π–Π stacking maximum length of PDI self-assembly may extend to a micrometer level, which favors the Π-electron transfer and thus enhances photoconductivity of the materials, i.e. ultralong nanobelt self-assembly (Fig. 2(f))[98] and ultrathin n-type organic nanoribbons (Fig. 2(g))[106] under strong Π–Π stacking interaction. In addition, PDI molecules as hydrophobic subunit can be covalently coupled with another hydrophilic subunit to form amphiphilic molecules with a more controllable assembly ability[107].

4. Electronic structure of PDI self-assembly

4.1. Identification of band-like electronic structure of PDI self-assembly

The PDI molecule belongs to a type of dye whose energy level gap measured by UV–vis absorption spectra corresponds to ca. 2.5 eV, similar with the theoretical value calculated through DFT calculations. The light adsorption of PDI originates from perylene chromophore, and the polarity of cyclic amide leads to the red-shift of absorption peak. Hence, its frontier orbital energy levels consist of the orbital correlation of C and O atoms in the two units. Generally, there exists three different electronic transition modes for monomeric PDI molecules, and thus three corresponding characteristic absorption (400–550 nm) and emission peaks shown up in UV–vis absorption and fluorescence spectra, respectively. According to DFT calculations, the energy levels of the frontier orbits of parent PDI molecules are positioned at –6.11 eV (LUMO) and –3.57 eV (HOMO). The PDI molecule structure does not deliver continuous electronic energy band structure, since only the crystals form band-like electronic structures. The band gap of PDI self-assembly is dependent upon the packing degree and length in PDI self-assembly with PDI

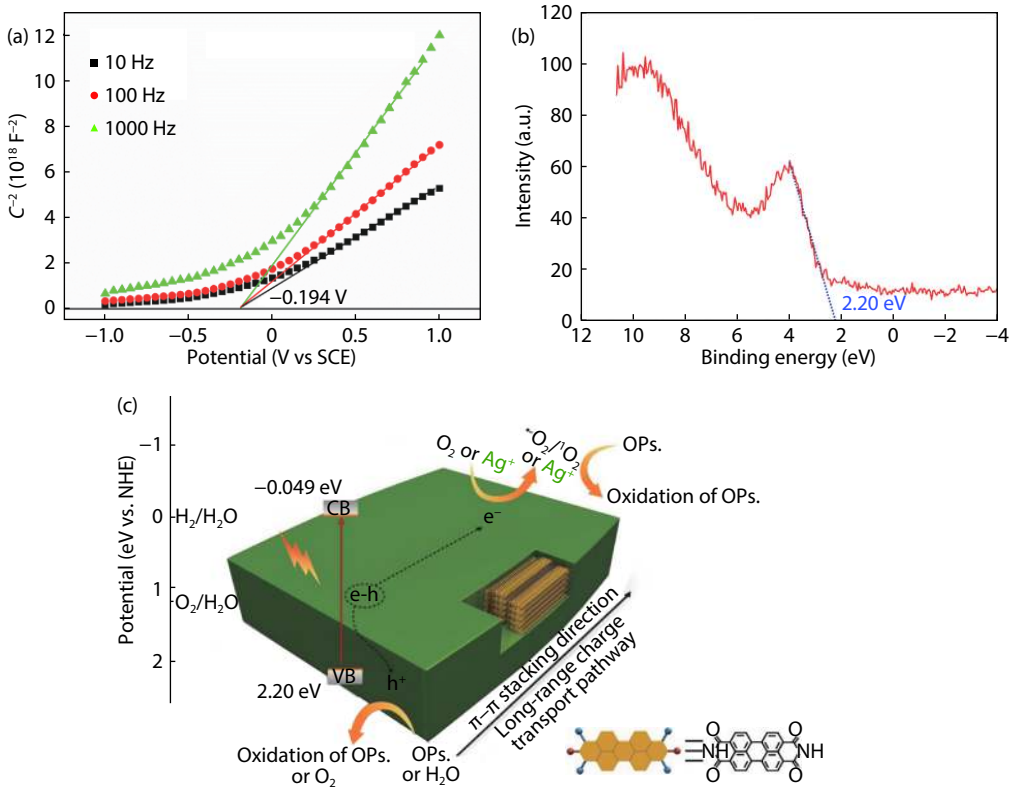

Fig. 3. (Color online) (a) Mott–Schottky curves and (b) XPS valence-band spectrum of the self-assembled PDI supramolecular system. (c) Schematic illustration of the electronic energy level structure of PDI self-assembly with permission from Ref. [64].

molecules as building blocks[74]. This case can be analogue to the reported one-dimensional poly(diphenylbutadiyne) nanostructures[32], and its electronic structure greatly hinges on the length of the conjugated polymer. The longer the conjugated chain of the conductive polymer, the narrower the corresponding energy band gap and thus the wider the visible-light absorption range. DFT calculations displayed that through Π–Π stacking, the continuous energy levels of PDI self-assembly are consequently formed with lowered absolute energy levels of HOMO and LUMO, different from discrete energy levels of individual PDI molecule[74]. Compared with PDI molecules, the characteristic absorption peak of PDI self-assembly is red-shifted, which is located at ca. 550 nm, because of the orbital overlapping between PDI molecules. By means of absorption spectrum, the Mott–Schottky curve (Fig. 3(a)) and X-ray photoelectron spectra (XPS) (Fig. 3(b)), Liu *et al.* estimated the CB and VB potentials of PDI self-assembly at –0.049 and 2.20 eV, respectively[64]. The flat-band potential given by the Mott–Schottky curve is –0.194 V versus SCE. According to the difference between the flat-band potential and the CB potential of n-type semiconductors by 0.1–0.2 eV[108], the CB potential can be gauged to be –0.049 eV, higher than LUMO levels of the isolated PDI molecules. Moreover, from the XPS valence-band spectrum, the VB potential of the PDI self-assembly is analyzed to be about 2.20 eV. Such deep VB position is sufficient to thermodynamically facilitate photocatalytic oxygen production (Fig. 3(c)). The formation of the band-like electronic structure stems from the ordered self-assembly structure generated by the Π–Π stacking behavior of PDI molecules. In view of the unique electronic structure of PDI self-assembly, PDI self-assembly-based materials have been deployed in organic optoelectronic device manufacturing and solar cells[109–114].

4.2. Approaches to tune the energy bands of PDI self-assembly

With an aim of purposeful utilization of the sunlight and improvement of photocatalytic redox reactions, regulating electronic energy bands of semiconductors is critical and effective. For example, narrowing energy band gap can extend light absorption range to the entire visible-light wavelength so as to efficiently utilize the solar energy as far as possible; adjusting the CB and VB position can make it possible to reach the potentials required for redox reactions and initiate overall reaction kinetics. In theory, for photocatalytic water splitting, when the potentials of CBs approach 0.5 to –1.5 V vs. NHE, the semiconductors can photocatalyze water into H_2; and if the VB potentials reach 1.0–3.5 V vs. NHE, the semiconductors perform a strong capability to realize water oxidation[6]. For photocatalytic degradation, the potential relationship between the CB/VB of semiconductors and $O_2/O_2^{-}\cdot$ or $H_2O/OH\cdot$ needs to be considered for photocatalytic conversion and mineralization, because the main redox active species in photocatalytic degradation are holes, superoxide radicals and hydroxyl radicals[8, 64, 115]. For inorganic semiconductors, the electronic structure can be controlled via surface doping[116–120] and surface defects[121–125]. The electronic structure of an organic semiconductor is relevant to its own composition and construction as well. Unlike inorganic semiconductors, the structure of organic semiconductors is constructed by a variety of constituent units with varied numbers of building blocks or arrangement patterns. Different units in an organic semiconductor present different electronic structures. In addition, since the aggregation process of PDI self-as-

sembly is a dynamic equilibrium process between gel and sol, it is greatly affected by external conditions[73, 76]. This also induces drastic change in electronic structures of PDI self-assembly. For instance, during photocatalytic degradation, because of the accumulation of photogenerated charges in PDI self-assembly, it would disaggregate gradually and thus reduce its photocatalytic performance. But PDI molecular structure is photochemically stable and would not dissociate under irradiation. The possible strategies are summarized as the following for adjusting electronic structures of PDI self-assembly: (1) Modifying isolated PDI molecule structures; (2) Tuning Π–Π stacking arrays via side-chain substitution; (3) Combining with other materials; (4) Utilizing PDI anion/dianion radicals.

4.2.1. Electronic modification of isolated PDI molecules

4.2.1.1. Substitutions at Π-conjugated perylene fragment

Modification to bay areas of PDI molecules with electron-defective or electron-rich substituents is an effective approach to adjust electronic structures of isolated PDI molecules and follow-up PDI self-assembly. The approach is firstly mastered by Seybold *et al.*, via incorporating four phenoxy groups to substituted chlorine groups at bay positions[126]. The perylene ring with chlorination has been reported albeit not excluding a mixture existence of three- or five-fold chlorination by-products[127]. Although the mixture of bromination PDI is obviously worse than that of chlorination PDI, the derivatives initiated from it on can be used to yield some PDI molecules with functional group modification at bay areas, including carbon, cyano[128], oxygen and nitrogen[129, 130] nucleophiles. Substitution at bay areas via conventional organic synthesis is rather unsatisfied due to sluggish reactivity and a lack of chemoselectivity. Fortunately, photocatalytic and electrochemical organic synthesis, as an effective, safe and facile catalytic protocol, have aroused increasing attention in recent years owing to mild reaction conditions, highly economic atom utilization, sustainable energy consumption and high chemoselectivity[131–135], to provide another possibility for substitution at perylene rings. For example, aromatic C–H/cyclohexylamine N–H coupling can occur with a high yield and selectivity under irradiation[133]; aromatic C–H amination with secondary amines has been reported by using the appropriate current as an oxidant agent[136]. These synthetic tools are believed to be very useful for modification of organic materials, hence some excellent related references are provided here to broaden our synthetic horizons[137–146]. Undoubtedly, installation of an alkyl group at perylene rings can improve PDI solubility. Additionally, modification to perylene rings would affect PDI self-assembled arrangements since perylene rings are twisted more seriously originated from steric hindrance of substituents[95, 96], and consequently change its supramolecular structures/morphologies. For instance, Ke and coworkers designed two types of molecular building blocks at the bay area forming totally distinct nanostructures: plate-forming system and nanosphere[71]. Krieg *et al.* proposed an idea that a perfluorooctyl chain attached to the perylene ring can dramatically increase the strength of supramolecular bonding in aqueous environments, giving rise to exceptionally strong noncovalent binding[147]. More importantly, this type of modification would greatly influence the electronic and optical properties of PDI molecules[148]. This technology is broadly applied in the field of solar cells, rendering sunlight utilization of PDI-based materials to be further enhanced. For example, dimeric PDI material was synthesized to obtain energetically deep HOMO and LUMO levels, thus giving a high solar conversion efficiency of 2.21%, and N-alkyl chain modification at the bay area made it increase to 3.13%[149]. Li and coworkers fabricated a large BN-embedded Π-system based on PDI molecules to improve its optical characteristics[150]. For more specific synthesis of PDI derivatives, Marder group's review in 2011s can be referenced, which details the substituent modification to various types of PDI derivatives[92].

4.2.1.2. The change in electronic structure of PDI molecules

The modification to bay areas of PDI molecules cannot only modify electronic energy levels of PDI molecules, but also transform Π–Π stacking arrangements in PDI self-assembly. Both of these would lead to the change in electronic structures of PDI self-assembly. When electron-withdrawing or electron-donating groups are introduced into perylene bays of PDI molecules, the substituents electronically interact with PDI molecular orbital, causing the charge density redistribution in PDI molecules, which influences LUMO and HOMO levels of PDI molecules. In electrochemical measurements, PDI molecules undergo a transformation in three types of existent states (PDI, PDI^{-} and PDI^{2-}), and hence the reduction potentials of PDI molecules can be observed (Fig. 4(a)). Seifert *et al.* found out via electrochemical measurements that two reversible reduction peaks of highly electron-deficient PDI shifted to a more positive potential, and the reduction potentials of the PDI derivatives with substituents at the bays were compared as following: Cl_4PDI > Br_4Cl_4PDI > $(CN)_4Cl_4PDI$[151]. Fig. 4(b) showed the redox potential difference between Br_4Cl_4PDI and $(CN)_4Cl_4PDI$. In contrast to electron-deficient substituents, linking perylene motif of PDI molecule with electron-rich substituents would decrease its ionization potential and electron affinity[149]. In order to obtain degenerated LUMO level, it has been reported that the perylene bays of two PDI molecules can be connected through fulvalene[154]. The integration of bi-element X–Y unit (e.g. N-B) with obvious electronegativity difference would cause a great change in molecular frontier orbitals[150]. In addition, the gap of the electronic energy levels of PDI molecules can also differ in the types of introduced functional groups[91]. Schuster *et al.* prepared PDI molecules linking with double-[6] helicene and constructed helical nanoribbon with these molecules as building blocks. As a tool for investigating three-dimensional structures and electronic structures of supramolecules, the circular dichroism revealed that the rigid double-[6] helicene substructure resulted in the larger molar electronic circular dichroism in the nanoribbon WH[6][6] relative to the smaller analogue WH[6], increasing by a factor of 5. As the size of the helical nanoribbon decreased, the electronic circular dichroism declined due to the difference in electronic structures, though the profile and intensity in the UV-vis absorbance spectra are nearly similar (Figs. 4(c) and 4(d))[152]. The trapping effect of charge carriers in PDI molecules can be influenced by substituents at bay areas, which determines reduction potentials of PDI molecules[155].

In addition, increasing the degree of Π-conjugation of

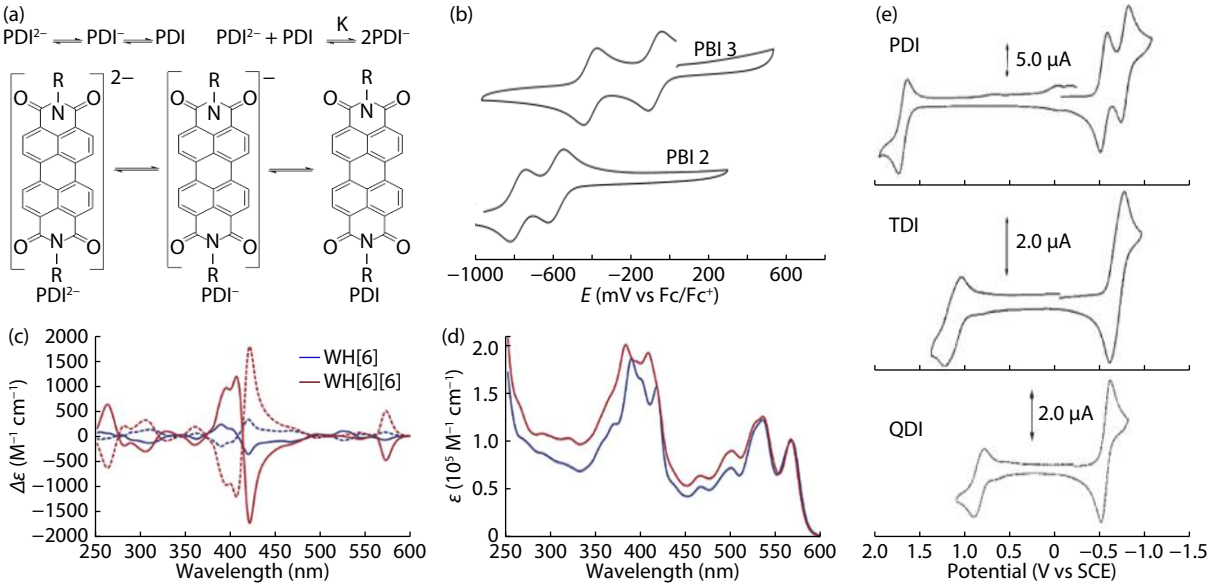

Fig. 4. (Color online) (a) Schematic representation of the equilibrium between reduced form (PDI^{2-}), intermediate (PDI^{-}) and fully oxidized form (PDI). (b) Cyclic voltammograms of Br_4Cl_4PDI (PDI 2) and $(CN)_4Cl_4PDI$ (PDI 3) in dichloromethane with permission from Ref. [151]. (c) Electronic circular dichroism, (b) UV-vis absorbance of WH[6] and WH[6][6] in dichloromethane (10^{-6} M, 1 cm path length) at room temperature with permission from Ref. [152]. (e) Cyclic voltammograms of 0.8 mM PDI in $CHCl_3$/MeCN (3 : 2, v/v), 0.21 mM TDI in $CHCl_3$/MeCN (4 : 1, v/v), and 0.1 mM QDI in $CHCl_3$/MeCN (4 : 1, v/v). Scan rate: 0.5 V/s (electrolyte: 0.1 M $TBAPF_6$) with permission from Ref. [153].

aromatic rings can also effectively tune electronic structures of PDI anlogues. The perylene ring of PDI molecules was expanded by Lee *et al.* to obtain terrylenetetracarboxylic diimide (TDI), and quaterrylenecarboxylic diimide (QDI) counterparts[153]. Interestingly, it was found that the first reduction potential shifted less negatively and the oxidation potential moved toward less positive direction with the aromatic core expansion, in line with the calculated orbital energies (Fig. 4(e)). Moreover, the reduction of TDI and QDI can be considered as the two-electron exchange process accounting for the presence of only a single reduction wave. In 2018, Peurifoy *et al.* designed three-dimensional graphene nanostructures with PDI as one of structural units, which demonstrated an improvement in absorption and the electron-extracting effect[156]. A three-dimensional spiro-fused PDI molecules were prepared by Wang's research group with a high semiconducting performance[157]. They found that spiroconjugation structure induced the red-shift in absorbance. Meanwhile, the broadened and intensive absorption and aligned LUMO levels were observed. The integration of the conjugated subunits in the perylene bay of PDI cannot only expand the absorption range, but also form the subtle configuration (e.g. the superhelical structure)[158]. For such structures, LUMO is dominantly located in the PDI core, and the substitution unit would greatly affect HOMO and subsequent occupied molecular orbitals.

4.2.2. Tuning PDI self-assembled array via side-chain substituents

4.2.2.1. Various modifiability of side-chain amides

Suitable substituents introduced at imide nitrogen of PDI molecules are necessary for controlling the self-assembled process to obtain desirable well-defined supramolecular structures. It is not only because substituents provide H-bonds/side-to-side chain interactions for lateral growth of PDI self-assembly, but also sterically hindered counterparts would weaken Π–Π stacking interaction between perylene rings, permitting a pathway-controlled self-assembly. For example, PDI-$[GY]_2$ (GY = glycine-tyrosine) forms chiral nanofibers while PDI-$[GD]_2$ (GD = glycine-aspartic acid) aggregates into spherical morphology, which depends on the nature of substituents at side chains[73]; side-chain substituents can control specific morphology of PDI self-assembly, e.g. one-dimensional nanobelts vs. zero-dimensional nanoparticles because of the sterically hindered effect of side-chain substituents on Π–Π stacking structure of PDI self-assembly[72]. The synthetic approach is readily accessible via the reaction of commercially available PTCAD and a multitude of aromatic/aliphatic primary amines firstly developed by Langhals (Schemes 1(a) and 1(b))[159]. It is worth noting that with regard to the reactions between aromatic primary amines and PTCAD, Lewis acid is necessarily required as a catalyst to drive the reactions, such as $Zn(OAc)_2$. Typically, preparation of symmetric PDI molecules is using quinoline or iminazole as the suspending solvent by heating at high temperatures. In fact, quinoline is rather difficult to remove completely because of its insolubility in most liquid media, while iminazole needs to preheat to a certain temperature due to its high melting point (~90 °C), which sometimes makes chemically unstable amine reactants oxidize. Besides of symmetric PDI, Che *et al.* designed an asymmetric PDI with two different side chains to tune morphology of PDI self-assembly (Scheme 1(c))[98]. Moreover, they presented a new approach of constructing nanofibril heterojunctions of asymmetric donor–acceptor (PDI) dyad coupled with a long alkyl chain to achieve high photoconductivity with fast photoresponse (Scheme 1(d))[99]. Additionally, the side chains can also couple with metal ions (Zn^{2+}), together with Π–Π stacking interaction, to promote and stabilize PDI self-assembly[16]. Interestingly, some more complex molecular structures based on PDI have been designed aiming at the substituents of side chains. For example,

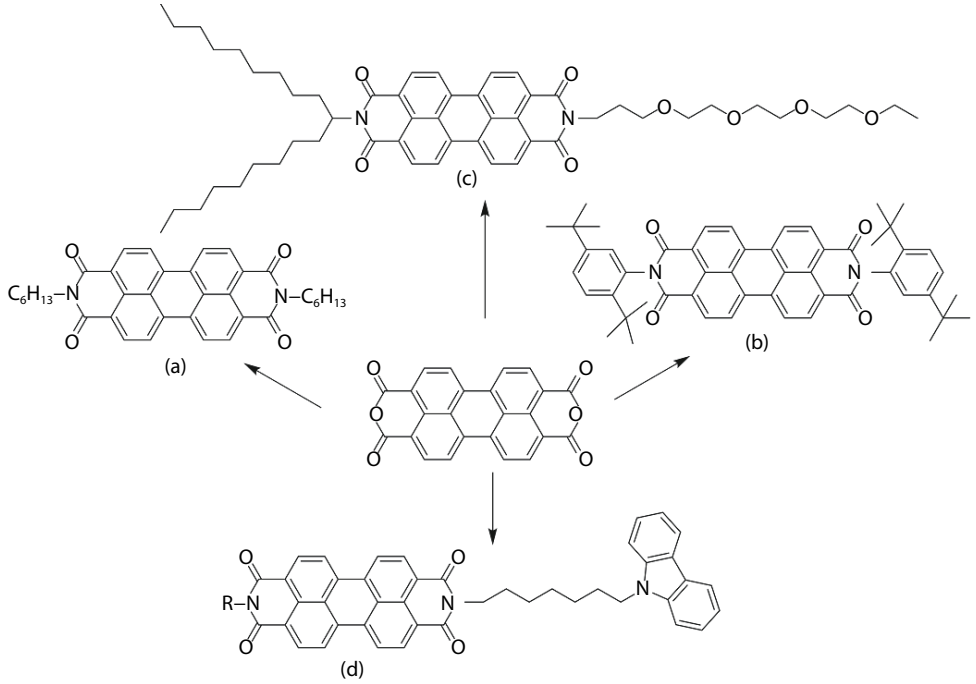

Scheme 1. Symmetric and asymmetric structures of PDI molecules.

Wang *et al.* successfully synthesized PDI macrocyclic dimer and a concatenated dimer-dimer ring from dynamic molecular self-assembly of monomeric bis-N,N′-(2-(2-(2-(2-thioacetylethoxy)ethoxy)ethoxy)ethyl) PDI[160]. And Beer's group constructed a large central macrocycle consisting of a PDI unit and two triazolium anion-binding motifs via an anion template synthetic method[161].

4.2.2.2. Preparation of PDI self-assembly for photocatalytic applications

Current methods for preparing PDI self-assemblies are various, generally including substrate-supported in situ self-assembly, solvent-phase interfacial self-assembly, vapor-triggered self-assembly at the interface of solid/gas or liquid/gas systems, pH triggered self-assembly in aqueous solution, and chemical reaction-mediated self-assembly of unsubstituted PTCDA and perylene diimide, etc.[91]. One commonly used access to PDI self-assembly is solvent-phase interfacial self-assembly (Fig. 5(a)). The basic principle of this method is to optimize the stacking structure of PDI self-assembly via adjusting binary solvent components (good and poor solvents) and some environmental factors (e.g. temperature, concentration, pH)[80]. Nonetheless, the preparative amount of PDI self-assembly using some of the approaches is only a few milligrams, which is difficult to handle on practical preparation of photocatalysts because the amount of photocatalysts required for academia is routinely several hundred milligrams, and that required for industrial production is much greater. As discussed above, parent PDI is not readily dissolved in most of solvents due to strong Π–Π stacking interaction unless some substituents are introduced into side chains to overcome a high barrier of uncoupling two PDI molecules through the strong interaction between solvent and PDI. PDI self-assembly can be regarded as a supramolecular, and thereby two definitions (good and poor solvent) in supramolecular field can be employed in PDI self-assembly to elaborate its solubility in some solvents. A good solvent is a type of solvent that possesses strong dissolving power for the supramolecular with the interaction parameter χ for supramolecular of less than 0.5, on the contrast of poor solvent that is conducive to Π–Π stacking and side-to-side chain interactions. Some organic solvents have been adopted to dissolve a small amount of PDI molecules, such as $CHCl_3$, DMF and DMSO. In view of g-C_3N_4 preparation method whereby concentrated H_2SO_4 solution can act as intercalator to separate C_3N_4 sheet layers from bulk C_3N_4[163], PDI molecules can be easily dissolved in concentrated H_2SO_4 solution, and nearly gram-level dissolution per milliliter was successfully realized to construct desired self-assembly photocatalysts (Figs. 5(b) and 5(c))[19, 64, 74]. This method enables realization of PDI self-assembly with highly ordered Π–Π stacking structure more feasibly with the subsequent addition of distilled water as the poor solvent. If side-chain substituents contain some acidic functional groups, such as carboxyl acid, PDI molecules can be dissolved in alkaline solution followed by neutralization with diluted acid to initiate PDI self-assembly[74]. Besides, modified PDI molecules by specific substituents turns out to be increasingly soluble in organic solvents according to the rule of the likes dissolve each other. For example, polyoxyethylene side-chain attachment in PDI leaves it dissoluble in alcohol, and tuning the volume ratio of alcohol and water can effectively control the formation of ultralong nanobelts[98]. The flexibility of the propoxyethyl substituents at the side chains endowed PDI more solubility in chloroform but insoluble in methanol. According to this, injecting concentrated chloroform solution of PDI into methanol facilitated formation of the highly ordered PDI self-assembly[75]. Therefore, for PDI molecules with oxidatively labile or acid-susceptible functionalities, it may be considered to introduce more lipophilic substituents to enhance solubility in organic solvents.

Alternatively, another possible approach is metal-ligand-coordination (Fig. 5(a)). Zeng *et al.* fabricated the single crystalline metal-organic polymer based on PDI self-assembly using

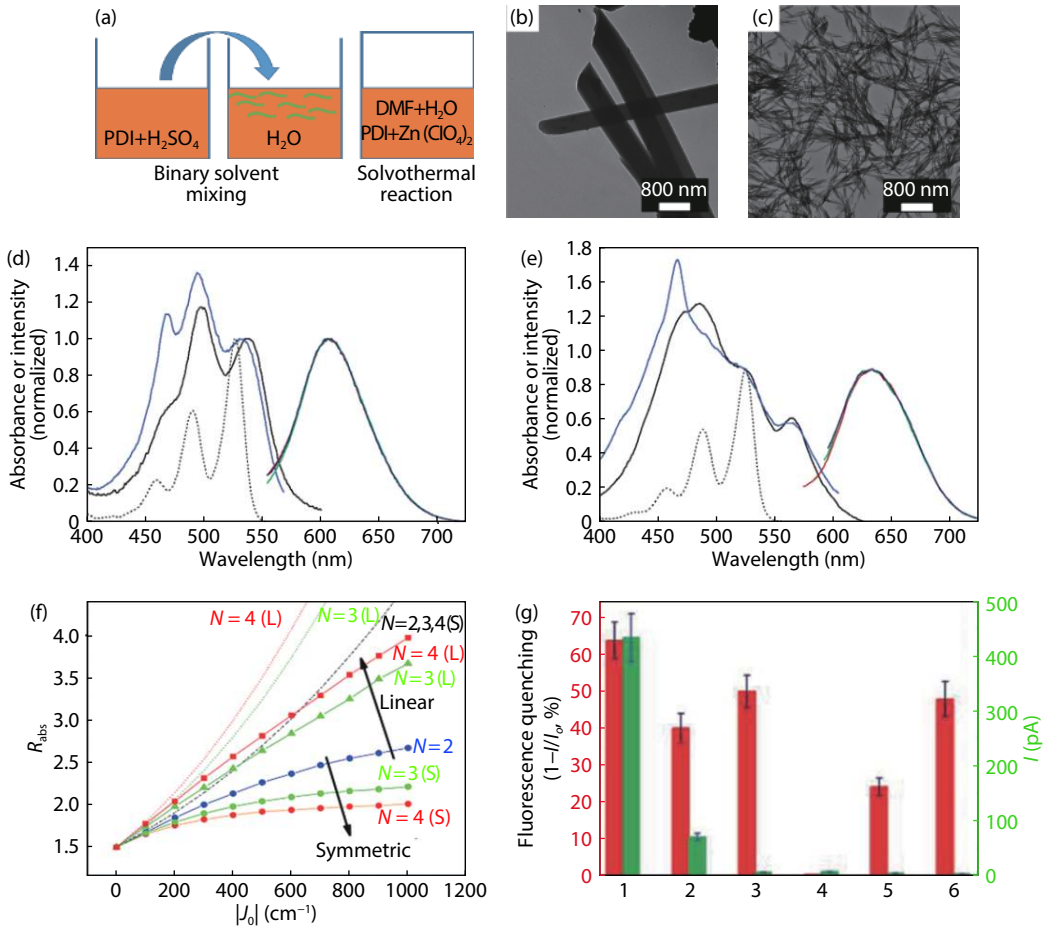

Fig. 5. (Color online) (a) Diagrams showing the approaches relative to binary solvent mixing and metal-ligand-coordination-directed method. TEM images of (b) bulk PDI and (c) nano PDI with permission from Ref. [74]. UV–vis absorption (black) and fluorescence excitation (blue) and emission spectra of a thin film of (d) ND-PDI and (e) DD-PDI spin-cast on glass from a chloroform solution with permission from Ref. [72]. (f) Calculated ratio of 0–0 and 1–0 oscillator strengths for the linear and symmetric series as a function of $|J_0|$ using $\lambda_2 = 0.60$ with permission from Ref. [162]. (g) Comparison of optical and electrical performance between various D/A heterojunctions with permission from Ref. [99]. The red and green columns denote fluorescence quenching and photocurrent measurement, respectively.

this method[16]. Via hydrothermal reaction, the final PDI-Zn^{2+} coupling photocatalyst was obtained by using bis(N-carboxymethyl) perylene imide as the ligand and $Zn(ClO_4)_2{\cdot}6H_2O$ as the metal-ion coupling agents. The key point of the PDI structure is with substituents of carboxyl acid, providing coupling sites for Zn^{2+}. On the other hand, alkaline side-chain substituents can also be used to coordinate metal ions. For example, using pyridine/terpyridine receptors to coordinate with Pt(II), Pd(II) or Zn(II) ions is a feasible strategy to drive PDI self-assembled process. This method can be deployed to prepare cyclic polymers consisted of four PDI molecules and metal ions[164]. With the ferrocenyl-substituted N,N′-di(4-pyridyl) PDI as the ligands and the complex [Pt(dppp)][$(OTf)_2$] as angular building blocks for the metal-mediated self-assembly, the self-assembled supramolecular was constructed with 90° corner in the square supramolecular structure.

4.2.2.3. Side-chain effect on electronic structure

Though side chains at the nodes of PDI molecules do not obviously alter electronic structures of PDI molecules, it can modulate Π–Π stacking modes of PDI self-assembly, thereby acting on its electronic structure, which has been verified via DFT calculations using a series of PDI self-assemblies with different side-chain substituents[165]. Zang's group introduced substituents with different steric hindrance at the side chains, exhibiting different light absorption properties[72], namely, their electronic structures are totally different. Relative to the absorption spectrum, the higher transition in ND-PDI at the shorter wavelength was exhibited in the excitation spectrum (Fig. 5(d)). Moreover, the emission at the excitation of the longer wavelength declined, possibly due to the symmetry-forbidden relaxation transition from the lowest-energy excited state to the ground state[68]. Interestingly, though in homogeneous solutions, the absorption and emission spectra of ND-PDI and DD-PDI were nearly approximate which resulted from the similar PDI skeletons, the corresponding emission peak of DD-PDI self-assembly was red-shifted by 30 nm related with that of ND-PDI self-assembly centered at 605 nm (Fig. 5(e)), mainly because of the stronger Π–Π stacking interaction. The strong interaction led to the significant decrease in the emission quantum efficiency in line with the enhanced characteristic absorption band originated from Π–Π stacking interaction. PDI self-assemblies with different nanosizes also partly determine different electronic features, e.g. PDI nanowires and nanoribbons[74, 166]. The difference arises from the change in the Π–Π packing degree between the PDI molecules within the PDI self-assembly units. Normally, H- and J-type behaviors are the main aggregation forms of PDI self-assembly via tuning side-chain substituents, and display differ-

ent electronic structures[19, 104]. In 2013, Spano's group prepared a symmetric star-shaped complex composed of three PDI molecule subunits by "head-to-tail" linking way at the cyclic amide N. Unlike the "head-to-tail" linear complex with J-aggregate behavior, the star-shaped complex exhibited a unique photophysical response different from H- and J-type, e.g. absorption/emission polarized direction, red-shift of the 0–0 peak with increasing $|J_0|$, initial linear rise of the 0–0/1–0 oscillator strength ratio with increasing $|J_0|$ (Fig. 5(f)), and radiative decay rate[162].

The PDI molecules can act as electron acceptors that can exchange electrons with some other molecules/materials with electron-donating capability. This interaction can effectively regulate the conduction of photo-generated charges in PDI self-assembly[154, 167, 168]. The conduction of electrons to PDI as well as the transfer of holes to the counterpart enables photoinduced electrons and holes to be separated, enhancing intra/intermolecular charge transportation. Doessel *et al*. constructed covalently linked hexa-peri-hexa benzocoronene (HBC)/PDI dyads which self-assemble into well-ordered two-dimensional supramolecular structures with the cross-stacking of the HBC and PDI motifs[169]. The steady state fluorescence spectra demonstrated rapid exciton transfer from the HBC unit to the PDI unit through Förster-type fluorescence resonance energy transfer. The nano segregated stacking of HBC and PDI with sufficient orbital overlap promoted photoinduced electron transfer between HBC and PDI through charge transport channels. Besides, Jiang's group constructed donor–acceptor super heterojunctions to promote charge separation, transfer and collection via the covalent incorporation of metallophthalocyanines and PDI. In this periodically ordered supramolecular structure, a pair of metallophthalocyanine donor and diimide acceptor were interacted directly forming molecular interface, which yielded a long-life charge separation state[170]. For the structure D–A–D type, under the irradiation of a certain wavelength, D and A undergo electron transfer to form D^+–A^-–D or D^+–A^{2-}–D^+ charge separation states, where the charge separation rate constant is much greater than that of charge recombination, e.g. a classic system containing PDI and two porphyrin moieties[130, 171–173]. PDI anion/dianion radicals play a critical role in stabilizing charge separation states[173]. Aside from the formation of donor–acceptor dimers linked by covalent bonds, non-covalently linked dimers can also be constructed for the purpose. For example, 7,7,8,8-tetracyanoquinodimethane and PDI self-assembly were utilized as the electron acceptor and electron donor, respectively, realizing effective charge separation and thus improving photocatalytic performance[86]. The prepared dimers exhibited different light absorption properties from pure PDI self-assembly. Via interfacial engineering, an electron donor (D) was coated on PDI electron acceptor (A) by Zang's research group to fabricate the D/A heterojunction[99]. At the large D/A interface, photoinduced charge spatial separation was facilitated. Various D/A heterojunctions led to different optical and electrical performances (Fig. 5(g)). Compared with PDI self-assembly with the smaller skeleton in donor units, PDI self-assembly with the larger alkyl borne of donor units demonstrated six-fold higher photocurrent and 1.5-fold fluorescence quenching efficiency. A large enough donor skeleton in size can interact with PDI more effectively because of stronger interfacial and electronic interactions. To further suggest the effect of side chains on interfacial D/A interface, the donors bearing short, more hydrophilic side-chains was fabricated to construct new D/A interface with PDI. As expected, a separated interface formed consequently, largely inhibiting the electron-transfer interaction at the D/A interface as verified by the experimental results of neither fluorescence quenching nor photocurrent generation for this type of D/A interface (Fig. 5(h)). This suggests that D/A interfacial interaction can affect the electronic structure of the aggregate systems. However, due to bulk stacking of mixed phases from electron-acceptors and donors, a rapid charge recombination may take place along with the loss of energy[106].

4.2.3. Combining with other materials

4.2.3.1. Preparation of composites for PDI aggregate on the surface

The construction of PDI self-assembly-based composites can be employed for the modification of electronic structure of PDI self-assembly. The Π–Π stacking interaction between PDI molecules is usually much stronger than the interaction between PDI molecules and supporting materials, unless the template is modified with appropriate polar groups so as to build a strong coupling effect with functional groups of PDI molecules. Adsorption of a few PDI molecules on templates favors connection of more PDI molecules and follow-up formation of PDI self-assembly on the surface. Via pH-induced aggregation, PDI self-assembly can be loaded on the surface of inorganic semiconductor nanoparticles, forming the core-shell structure[8]. Using the Π–Π stacking interaction between PDI molecules and carbon materials, we can also allow PDI self-assembly to firmly connect with carbon materials to obtain highly stable self-assembled composites[82, 85]. However, this type of method may cause the change in the Π–Π stacking arrangements between PDI molecules, which may drastically affect photocatalytic performance of PDI self-assembly because photogenerated charge-transfer mode along the Π–Π stacking direction may be changed. Some PDI molecules containing polar functional groups (–COOH) would interact strongly with inorganic semiconductors, thereby destroying the ordered stacking structure of PDI self-assembly and leading to decayed photocatalytic kinetics[10].

4.2.3.2. Rebuilding the electronic structure of PDI self-assembly

Π–Π stacking permutations of PDI self-assembly are closely pertinent to external environments, mainly because the PDI self-assembly is a dynamic balance process between aggregation and disaggregation[174]. Substances with strong interaction with PDI self-assembly (such as surfactants) could change the packing structures of PDI aggregates[175]. Taking advantage of this common property of self-assembly, we can introduce a supporting material to enable a new stacking rearrangement of PDI self-assembly through the interaction with PDI molecules, so as to tune the electronic structure of PDI self-assembly. Wei *et al*. fabricated a PDI/P25 core-shell structure with P25 nanoparticles as the core and PDI self-assembly as the shell[8]. They found that the PDI self-assembly on the surface of P25 nanoparticles presented staggered Π–Π stacking and a dihedral angle due to interfacial strain. Compared with the long-range ordered structure of the pure PDI self-assembly, the PDI self-assembly attached to TiO_2 nano-

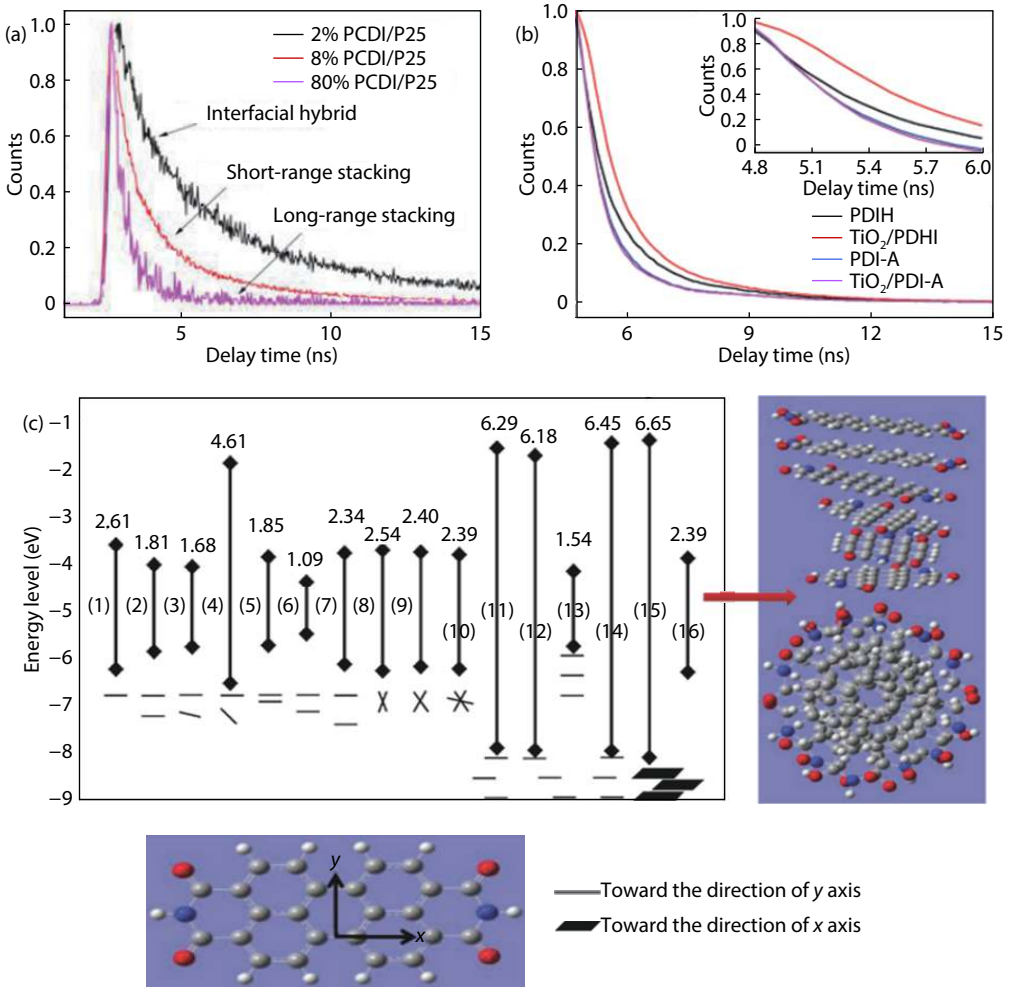

Fig. 6. (Color online) (a) Fluorescence decay transients measured at 470 nm for 2%, 8%, and 80% hybrids with permission from Ref. [8]. (b) Fluorescence decay transients measured at 450 nm for pure PDIH, PDI-A, TiO_2/PDIH, and TiO_2/PDI-A. (c) The energy levels based on different stacking arrangements between PDI molecules via DFT calculations with permission from Ref. [10].

particles corresponded to the short-range ordered structure. Generally, the transportation distance of electrons in organic semiconductors is within several hundred nanometers. If exceeding the distance, photogenerated electrons and holes are prone to recombine and annihilate, or deliver to some other surrounding chemicals. Therefore, the long-path transfer of photogenerated charges is not conducive to utilization of photogenerated charges for photocatalysis, whereas the short-range ordered structure can effectively prevent the recombination of photogenerated charges, albeit likely resulting suppressed charge carrier mobility by the defects[176]. The short-range Π–Π stacking structure with a longer fluorescence lifetime exhibits different optical property and electronic structure from the long-range ordered structure (Fig. 6(a)). The average fluorescence lifetime of the optimal Π–Π stacking structure corresponded to 21.154 ± 0.486 ns when fitted to a one-exponential function, which surpassed the fluorescence lifetime (10 ns) of the general dyestuff in aqueous solution[177], indicating the suppressed quenching of the excited states. In addition, the same group further constructed a core-shell structure with TiO_2 nanoparticles as the shell and PDI self-assembly (different PDI molecules from the former) as the core[10]. The photocatalytic efficiency has a bearing on the side chains of PDI. When the side chains of PDI contains a polar functional group such as –COOH, the composite exhibited reduced photocatalytic performance relative with the pure PDI self-assembly, because the strong interaction between the side chains of PDI and the surface –OH of TiO_2 severely disturbs the Π–Π stacking structure of PDI self-assembly, which was verified by Fourier transform infrared (FT-IR) and fluorescence transient spectra (Fig. 6(b)). Through DFT calculations, it can be known that different Π–Π stacking arrangements (the distance between PDI molecules, the contact area of PDI molecules, the dihedral angle of PDI molecules and the varied number of PDI molecules in one self-assembly unit) in PDI self-assembly exhibited different electronic energy levels (Fig. 6(c)). Besides, a series of inorganic or organic materials are introduced to upgrade electronic structures of PDI self-assemblies, e.g. MoS_2[178], zeolite[179], Si[180] and polyelectrolyte[181]. But PDI self-assembly using this method has an unpredictable Π–Π stacking arrangement, and the performance of as-prepared self-assembly materials may be largely affected by preparation conditions.

4.2.4. Electronic modulation role of PDI anion/dianion radicals

Since the PDI molecules act as an electron acceptor[182], it has been reported that PDI molecules can gain electrons to produce PDI anion/dianion radicals which own different electronic energy levels[17]. The electron affinities of the

monomers of self-assembly would determine the improvement of electronic structures for efficient light utilization[183, 184]. PDI anion radicals can also be used as active intermediates in photocatalytic reactions, promoting reaction progress, such as photocatalytic dehalogenation[17]. The study showed that PDI molecules can accept the electrons of triethylamines for generating PDI anion radicals. Compared with PDI neutral molecules, PDI anion radicals have a strong reducing ability, especially their excited states. Light-excited PDI self-assembly also promoted the formation of a small amount of PDI anion radicals and PDI cation radicals within PDI self-assembly[8]. The charge transfer between PDI molecules was assumed to be equivalent to a redox reaction based on the Marcus theory, and thus there would be some charged active intermediates. Spatially and electronically isolated radical anion and cation moieties would co-exist in well-arranged self-assembly with a large amount[185]. These active intermediates in PDI self-assembly contribute to the improvement of photocatalytic performance, because DFT calculations show that PDI anion radicals possess higher LUMO levels than PDI neutral molecules, that is, stronger reducing ability.

4.3. Electron/energy transfer in PDI self-assembly

In the process of electron transfer, the PDI molecules have very small reorganization energy (0.15 eV), which promotes the electron/energy transfer between PDI molecules/motifs and other chemical compounds/motifs under the built-in electric field. A series of multifunctional integrated systems with extended tetracationic cyclophane/PDI systems as different constituent units were successfully designed by Scheman's research group[186]. By means of the spectroscopic technique, it can be verified that different heterocycles affect the energy transfer from the extended tetracationic cyclophane to the PDI molecule. Ramos *et al.* synthesized two PDI-based symmetrical arrays linked with oligoaniline-aligo(p-phenylene vinylene) (OAn-OPV), wherein the electron transfer rate between OAn-OPV and PDI with a direct linkage is faster than that with a saturated spacer in the middle of the two segments[187]. Besides, Ryan *et al.* prepared highly charged supramolecular complexes consisting of cyclobis(4,4'-(1,4-phenylene)bispyridine-p-phenylene)tetrakis(chloride) (ExBox) and three PDI molecules[188]. The effective electron transfer from ExBox to PDIs can be observed. The molecular orbital overlapping enabled the electron/energy transfer process and, as a consequence, the electron-transfer system should generate one unit with positive charge and the other with negative charge which can be verified through transient adsorption/fluorescence spectra. In addition, the charge-transfer process was observed in $[Ru(II)(phen)_2(pPDIp)]^{2+}$ complex where $[Ru(II)(phen)_2]^{2+}$ was linked at the imides of PDI molecule to form charge-transfer state $[Ru(III)(phen)_2(pPDIp^{-\bullet})]$[189]. Likewise, the structural basis of facilitating the electron transfer along the longitudinal axis is the Π-orbital overlapping between PDI skeletons that favors Π-electron delocalization. Hence, the transfer of photogenerated charges within PDI self-assembly can be consummated adjustably by modifying the structure of PDI molecules. The carrier mobility of PDI molecules can be gauged via pulse-radiolysis time-resolved microwave conductivity, corresponding to 0.1 $cm^2V^{-1}s^{-1}$ for liquid crystalline phase, and 0.2 $cm^2V^{-1}s^{-1}$ in crystalline phase[102]. The charge-transfer feature inside PDI assembly allows the materials to be extensively deployed in highly selective and stable chemical sensing for a wide range of reducing gases and organic compounds (NH_3, NH_2-NH_2, etc.)[79, 80, 106, 190–192]. For example, ultrathin n-type PDI self-assembled nanoribbons were used as a highly efficient vapor sensing for nitro-based explosives, merely attributable to effective electron conduction in PDI self-assembly[106].

The charge-transfer event in photo-excited PDI self-assembly is roughly as following: firstly, under the visible-light irradiation, PDI self-assembly produces photogenerated electrons and holes, and the minimum excitation energy of photogenerated charges depends on the energy band gap of PDI self-assembly; secondly, due to the Π–Π stacking interaction between PDI molecules, photo-generated charges can be rapidly separated along the Π–Π stacking direction in PDI self-assembly. The fluorescence lifetime of these photogenerated charges in organic semiconductors is around 1–100 ns[8], hence the annihilation of photoinduced charges would inevitably happen during electron conduction process along the Π–Π stacking direction on account of inelastic collision. In addition, photogenerated electrons and holes would somewhat have a propensity to recombine inside PDI self-assembly, releasing energies as a form of fluorescence or heat, or photogenerated charges are delivered to other chemical substances (such as O_2), that is, the process of converting light energy into chemical energy. Aside from Π–Π stacking along the vertical axis, the orbitals of PDI molecules may also overlap in the other two directions, resulting in a probability of charge transverse conduction. Additionally, Nathaniel *et al.* sought to PDI-helicene homologs by linking perylene rings of two PDI molecules[193]. Because the Π-electron "clouds" of the two PDI subunits in this structure collided with each other, the structure exhibited an extended electron-transfer feature, realizing intra-molecular through-space electron delocalization.

Inspired by the Marcus principle, the charge transfer process is actually analogue to a redox process, the redox mechanism between PDI molecules has been adopted to explain the charge transfer mechanism inside PDI self-assembly (Fig. 7)[8]. The thermodynamic calculations of the reaction PDI + PDI → PDI^- + PDI^+ showed that the required Gibbs free energy for the redox reaction is exactly equal to the thermodynamic work applied to the system by the two absorbed photons, which was in agreement with the experiment, indicating that the interpretation has certain credibility. First, PDI self-assembly, excited by visible-light photons, can generate active intermediates-PDI anion radicals, which can be detected by fluorescence spectra and electrochemical measurements[151], especially for stable electron-withdrawing materials due to strong electron affinity[154]. Moreover, PDI intermediates can absorb a second photon to form excited PDI anion radicals which have a stronger reducing ability[17]. The intermediate exchanges electrons with the neighboring PDI neutral molecules, thereby forming another new PDI anion radical. By analogy, the electron transfer inside PDI self-assembly is completed along Π–Π stacking direction. The charge carrier mobility along PDI self-assembly is largely dependent upon PDI molecular conformation and PDI stacking modes. Ball *et al.* reported an integrated system with chiral, helical PDI ribbons incorporated into two macrocycles, and the electron mobility of *cis*-structure was increased by a factor of 4 compared with

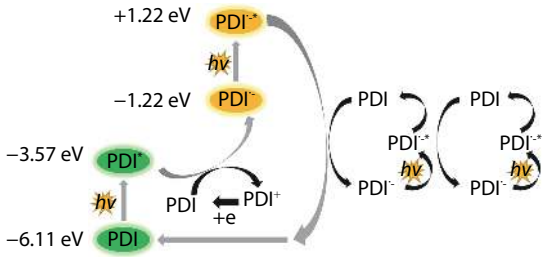

Fig. 7. (Color online) Proposed mechanism of electron transmission in PDI self-assembly, wherein the HOMO and LUMO levels are obtained via DFT calculations.

trans-structure[194]. Obvious differences in the lowest energy structures and strain energy between the cis-structure and trans-structure existed. Marcon *et al.* revealed that a twist angle between PDI molecules was conducive to hole transport via analyzing the relationship between charge mobility and stacking arrangement[176]. Well-overlapped PDI orbitals through Π–Π stacking interaction enables the ultrafast mobility of photogenerated charges in ordered columns[195].

Electron transfer along Π–Π stacking direction can smoothly proceed in a short range. Long-range electron conduction in the bulk may result in relative fast electron–hole recombination. The main reasons may be: a) the transfer of photogenerated electrons in PDI self-assembly is bidirectional, and thus electron conduction to a certain distance would inevitably terminate or shift in reverse direction; b) when PDI molecules are stacked to a certain extent, the subsequent stacking of PDI molecules cannot affect the electronic structure of PDI self-assembly.

In order to prevent the overly long Π–Π stacking dimension of PDI self-assembly, we could adopt some trade-off strategies on the basis of the crystal growth modes: (1) The common method is to change the side chains of PDI molecules, combined with the adjustment of the external environment, i.e., the side chains containing acidic/alkaline groups can be introduced for different acid-base equilibrium constants, followed by tuning the pH value of the solution to change its aggregation degree; as for the side chains with different lipophilicity/hydrophilicity, we can change the polarity of the mixed solvent to control the Π–Π stacking length. (2) As described above, building Π–Π stacking indentation inside PDI self-assembly is also an alternative method; (3) Appropriate templates/additives can be considered to control the growth rate or scale of PDI crystal nuclei.

5. Photocatalytic examples based on PDI self-assembly

5.1. Environmental remedy

5.1.1. Pure PDI self-assembly

PDI self-assembly is an efficient visible-light photocatalyst because it possesses appropriate electronic energy band structure, highly ordered Π–Π stacking structure, and strong adsorption interaction with organic compounds. The electron "clouds" of Π-orbits of PDI molecules overlap with each other, and this structure significantly narrows the energy band gap of PDI self-assembly, so that its light absorption range extends to the entire visible-light region. Due to the existence of molecular polar electric field, PDI molecules exhibit a high extinction coefficient, giving it a strong visible-light absorption ability. The Π–Π stacking structure of PDI self-assembly enables the rapid transfer of photo-generated carriers to realize spatial separation of photo-generated electrons and holes. The surface of nano-shaped PDI self-assembly has a strong adsorption effect on some negative ions in aqueous solution, hence the PDI self-assembly surface would be negatively charged and covered with hydration film[197] that makes it possible to deliver photoinduced charges to other chemical substances in photocatalytic reactions. As such, these organic supramolecular materials can be employed to photocatalytic degradation of organic pollutants. Liu *et al.* designed a willow-shaped supramolecular photocatalyst formed by the self-assembly of PDI molecules without side chains to achieve superior visible-light-driven catalytic degradation of phenol[64]. Its photocatalytic performance is more excellent than that of g-C_3N_4, BiOBr, $BiWO_4$ and commercial PDI, mainly due to expedient band-like electronic structure stemming from the Π–Π stacking alignment in the PDI self-assembly. The main active species for the photocatalytic degradation were found to be superoxide radicals, hydroxyl radicals and holes. They also investigated the detailed mechanism of phenol degradation on the generated intermediates-catechol and hydroquinone. Recently, another active species-H_2O_2 in PDI self-assembly systems has been found[198]. A series of structurally modified PDI self-assemblies were subsequently developed via tuning Π–Π stacking arrangement for photocatalytic degradation[19, 74]. Wang *et al.* upgraded an H-type PDI self-assembly with Π–Π stacking interaction and H-bonding as the driving forces for ordered self-assembly[74]. Due to the introduction of carboxyl groups at the side chains of PDI molecules, the H-type stacking arrangement was thus formed with the deepening of VB. The internal electric field in the PDI self-assembly promoted the separation of photogenerated carriers and improved the photocatalytic activity. Compared to the bulk PDI self-assembly, the VB and CB potentials (vs. NHE) of the nano PDI self-assembly both increased, thus leading to the rapid photocatalytic phenol decomposition. In addition, the overlapping degree of different PDI molecular orbitals in PDI self-assembly results in different photogenerated charge separation efficiency. The molecular orbital overlap in the H-type PDI self-assembly is larger, with the higher transfer efficiency of photogenerated charges; whereas the molecular orbital in the J-type PDI self-assembly can only partially overlap, reducing its photoelectric efficiency. Therefore, the photocatalytic oxidation ability of the H-type PDI self-assembly is stronger than that of the J-type PDI self-assembly (Fig. 8(a))[19]. Chen *et al.* utilized the PDI supramolecular nanofibers as the photocatalyst for degradation of ofloxacin and other fluoroquinolone abtibiotics[199]. The reactive species (h^+, $^1O_2$ and $\cdot O_2^-$) originated from photogenerated electrons and holes in PDI self-assembly play a crucial role in the photocatalysis. When the energy of the two localized excited states is lower than the energy of the charge-transfer state, the excitation of the two-component system can cause electron transfer between the components. Although the side-chain substituents hardly electronically interact with the PDI chromophore, the electron-acceptor and -donor units connected by a certain length of spacer in a molecule can also enable intramolecular charge transfer to yield a long-lived charge separation state as mentioned in Guldi's review on fullerene-porphyrin architec-

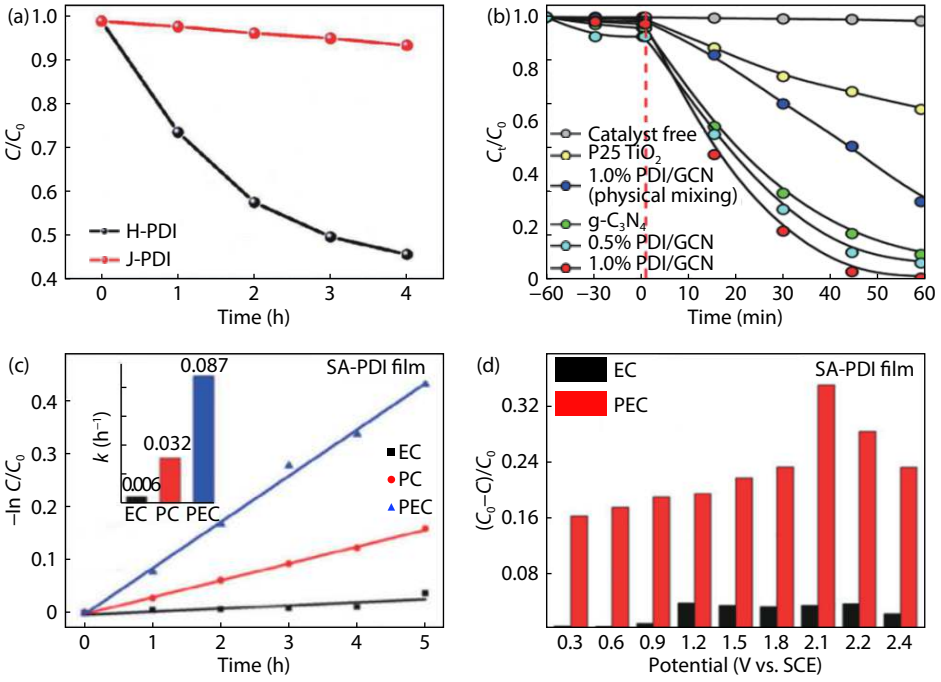

Fig. 8. (Color online) (a) Photodegradation curves for phenol (5 ppm) over H-PDI and J-PDI under visible light with permission from Ref. [19]. (b) Kinetics of photocatalytic degradation of an aqueous PNP under visible-light irradiating various PDI/GCN and reference catalysts with permission from Ref. [196]. (c) The first-order kinetics curve fitting for electrocatalytic (EC), photocatalytic (PC) and photoelectrocatalytic (PEC) degradation of phenol by the PDI film (visible light, 2.1 V applied voltage) with permission from Ref. [81]. (d) PEC and EC degradation of phenol (5 ppm) on the PDI film at various applied voltages in Na_2SO_4 solution (0.1 mol/L) with permission from Ref. [81].

tures[200]. Similarly, introducing an opportune molecular substituent that can exchange electrons with PDI at side chains of PDI molecules can facilitate the transfer of photo-generated charges between the side-chain substituents and PDI chromophore. Wang *et al.* fabricated a molecular heterojunction photocatalyst with a covalent linking of PDI and g-C_3N_4 for degradation of organic pollutants. The obtained superior performance was attributable to the photoinduced charge migration and separation through the heterojunction (Fig. 8(b))[196].

5.1.2. Composites

However, photogenerated charges in PDI self-assembly would also recombine and annihilate, severely corroding its photocatalytic activity. To boost visible-light photocatalytic activity of PDI self-assembly, some feasible approaches need to be developed. Composite photocatalysts based on PDI self-assembly are therefore developed to reduce the recombination of photogenerated charges. Wei *et al.* prepared the PDI/P25 core-shell structure, which greatly improved the photocatalytic activity of PDI self-assembly[8]. PDI acted as both dye sensitizer and photocatalyst. Two main factors have been proposed: (1) Formation of the short-range ordered structure in the PDI self-assembly reduced recombination of photogenerated electrons and holes; (2) Formation of electron channels at the interface between the PDI self-assembly and P25 promoted interfacial charge transfer. As the thickness of the PDI self-assembly shell changed, the composites demonstrated the different photocatalytic mechanism. Among them, the 22% PDI/P25 photocatalytic performance is the most prominent, benefiting from the synergy of PDI photosensitization and the photocatalysis of the PDI self-assembly. When the amount of PDI was less than 8%, the photosensitization of PDI played a major role in the photocatalytic process. In addition, the PDI/Pd@P25 ternary system was also constructed to further leverage its visible-light photocatalytic activity[9]. They assumed that the electrons in PDI self-assembly were transferred to Pd quantum dots, causing the energy of electrons in Pd quantum dots to rise, and then the electrons were back-transferred into PDI neutral molecules to form more active intermediates (PDI anion radicals), further promoting electron delocalization and enhanced photocatalytic activity. PDI anion radicals also facilitated interfacial charge transfer. As we know, PDI self-assembly can only utilize visible light, but the light absorption in UV region can only be emitted in the form of fluorescence, because the extremely active excited electrons make it easy to be quenched. The core-shell structure formed by TiO_2 nanoparticles coated with PDI self-assembly can hardly enhance the ultraviolet photocatalytic activity, probably because of the shielding effect of PDI self-assembly on ultraviolet light. Furthermore, to effectively harvest and convert the ultraviolet light, Wei *et al.* constructed a semi-core-shell structure of TiO_2/PDI self-assembly with PDI self-assembly as the core and TiO_2 nanoparticles as the shell[10]. The photocatalyst exhibited a full-spectrum photocatalytic performance. It was found that its light absorption extended to the near-infrared region, and the loading of TiO_2 nanoparticles on the PDI self-assembly played a key role in the broadening of light absorption. Under the interaction of interfacial electric field, the rapid transfer of photogenerated charge from the PDI self-assembly to TiO_2 further boosted its photocatalytic process. Another report on TiO_2 and PDI self-assembly is Cui's group, wherein they incorporated TiO_2 nanoparticles into the PDI self-assembly[201].

Besides of combination with TiO_2, composite construc-

tion of PDI self-assembly and other suitable materials (e.g. inorganic semiconductors, carbon materials, metal promoters) is also conducive to the improvement of photocatalytic performance. Yang *et al.* constructed p-Ag_2S/n-PDI composite materials to obtain a superior photocatalyst with full-spectrum utilization[83]. It was found that Ag_2S quantum dots contributed to the Π–Π stacking structure of the PDI self-assembly, thereby promoting the conduction of photogenerated charges along the Π–Π stacking direction. Moreover, the interfacial electric field between p-Ag_2S and the n-PDI self-assembly also accelerated the spatial separation of photogenerated electrons and holes, and effectively avoided the annihilation of photogenerated charges. PDI molecules can firmly adhere to multi-walled carbon nanotubes and graphene sheets via non-covalent interaction, making it excellently dispersible in aqueous solutions[202, 203]. At the same time, there is an obvious electronic coupling interaction between carbon materials and PDI in the hybriding form of the donor–acceptor[204]. Due to this effective Π–Π interaction, the combination of PDI self-assembly and graphene sheets formed a composite photocatalyst with better photocatalytic performance[82]. The synergistic effect of the PDI self-assembly and graphene sheets can be explained as the following: the rapid interfacial charge transfer between the PDI self-assembly and graphene sheets obviously decreased the recombination of photogenerated electrons and holes; graphene sheets with a large specific surface area possessed an outstanding enrichment effect on organic pollutants, and accelerated the kinetic process of photocatalytic degradation of organic pollutants. Likewise, C_{60}, as another kind of carbon material, also exhibits the photocatalytic auxiliary effect like graphene sheets. Wei *et al.* introduced C_{60} molecules on PDI self-assembly to accelerate the separation of photogenerated charges, and its photocatalytic degradation of phenol can be increased to 8.24 times compared with the pure PDI self-assembly[85]. The electron-withdrawing effect of C_{60} reduced the charge accumulation in the PDI self-assembly and favored the photochemical stability of the PDI self-assembly. It is worth nothing that for a hybrid of single wall carbon nanotubes (SWCN) and PDI self-assembly, the electron transfer from SWCN to PDI is also possible under excitation of a certain wavelength of light[205]. In addition, Miao *et al.* loaded Au quantum dots on PDI self-assembly, and acquired more excellent visible-light photocatalyst than the pure PDI self-assembly[84]. The surface plasmon resonance (SPR) effect of Au quantum dots was proposed for the enhancement of visible-light absorption. On the other hand, the lower Fermi level of Au quantum dots contributed to the photogenerated charge transfer from the PDI self-assembly to Au quantum dots. Zhang *et al.* constructed a supramolecular n–n heterojunction consisting of PDI self-assembly and Bi_2WO_6[206]. Their energy band positions were conducive to the rapid separation of photogenerated charges at the interface. The electrons in the CB of Bi_2WO_6 and the holes in the VB of the PDI self-assembly generated under charge-transfer interaction can accelerate the reaction kinetic process of photocatalytic degradation. An n–n type inorganic/organic heterojunction of flaky-like BiOCl/PDI photocatalyst was achieved by Ji *et al.* for photocatalytic degradation of cationic pollutants because of the electron transfer inside the PDI self-assembly and at the interface[207]. There is lots of research on PDI self-assembly-based photocatalysts for photocatalytic degradation, e.g. PDI/oxygen-doped g-C_3N_4[208], copper phthalocyanine/PDI[209], WO_3@Cu@PDI[210], PDI/PANI(Fe(III)-doped) heterostructure[211], PDI/BiOCl[212]. However, not all combination materials with PDI self-assembly can consummate PDI self-assembly-based photocatalysis. Some materials have a strong interaction effect with the structure of PDI self-assembly, which may destroy the Π–Π stacking structure of PDI self-assembly, so that the photo-generated charges cannot be effectively separated along Π–Π stacking direction. Furthermore, PDI molecules bearing strong polar functional groups also cause a stronger interaction with the surface –OH of inorganic semiconductors, and could distort the ordered Π–Π stacking structures. The potential difference of CB/VB between PDI self-assembly and other materials is another factor that needs to be considered because it can influence charge-transfer direction at the interface.

5.1.3. Photoelectrocatalysis

Photoelectrocatalysis is one of the most promising fields for our developing society to study how to effectively utilize the solar energy. Like traditional catalysts, the role of photocatalysts is to reduce the activation energy of the reaction and change the reaction pathway. Photoelectrocatalytic technology, as a new technology combined with photocatalysis and electrochemistry, has drawn increasing attention, along with the characteristics of photocatalysis and electrocatalysis[213–215]. Similar to photocatalysis, new mobile photogenerated carriers can be generated under irradiation. Furthermore, such charge carriers have a higher oxidation or reduction capacity than most carriers generated under electrocatalytic conditions in the absence of light. The excess energy of these minority photocarriers can be used to overcome a high barrier of electrocatalytic reaction, and even generate products that can store excess electron energy.

The effect of applied electric field further promotes the effective separation and transfer of photogenerated charges in photocatalysts. Since photogenerated electrons and holes are accompanied by equal amount, when they are in direct contact, simple recombination occurs consequently. This recombination leads to the phenomenon of short circuit galvanic cells on the surface of photocatalysts, which greatly reduces the efficiency of photon utilization. To effectively utilize the light energy and improve the efficiency of photocatalytic degradation, it is necessary to subject a positive potential bias to the catalyst electrode system. Zhu's group made their efforts to combine the photocatalysis of PDI self-assembly and applied electric field to achieve more robust photocatalytic performance compared with the photocatalytic and electrocatalytic processes (Fig. 8(c))[81]. The performance evaluation in Fig. 8(d) showed that when the applied voltage was 2.1 V, the photoelectrocatalytic degradation performance reached the optimal value. In the experiment, the ITO glass sheet covered by the PDI self-assembly was used as the working electrode (anode), while metal Pt as the counter electrode (cathode). Under the visible-light irradiation, a certain population of photogenerated electron–hole pairs were generated inside the PDI self-assembly. When a positive bias was applied to the PDI self-assembly electrode system, photogenerated electrons were induced to move toward the counter electrode. The direction of the electron migration is opposite to the direction of the current, thereby separating photogener-

ated electrons from holes, reducing or avoiding the probability of simple recombination. Thus, the lifetime of photogenerated hole in the PDI self-assembly can be prolonged. The photogenerated electrons transferred to the cathode participated in the formation of superoxide radicals. The holes residing in the PDI self-assembly promoted the formation of more hydroxyl radicals or directly participate in the degradation of phenol. Moreover, the electrode can act as a photocatalyst supporter, thereby somewhat avoiding separation of the photocatalyst after use, which simplifies the process of catalyst recycling. Additionally, the photocatalyst with PDI anchored to three-dimensional graphene was fabricated via simple electrodeposition-impregnation method[216]. The composite exhibited superior photoelectrocatalytic removal of organic pollutants due to the promoted separation and mobility of photogenerated carriers along the Π–Π stacking direction and adsorption-enrichment capability from graphene.

5.2. Energy production

5.2.1. O_2 evolution

Photocatalytic dioxygen production is a key scientific problem that needs to be solved urgently in the field of photocatalysis, mainly because dioxygen production acts as the decisive half-step for the overall water splitting reaction. The photocatalytic hydrolysis to produce dioxygen requires four electrons to participate in photocatalytic reactions, that is, the accumulation of holes on the heterogeneous photocatalyst, which determines photocatalytic reaction kinetics. Moreover, its overpotential is relatively higher, and often requires a lower VB potential to fit the requirement of water oxidation. It has been found that PDI self-assembly has a deep VB, higher than the oxidation potential of H_2O/O_2, and meanwhile the construction of PDI self-assembly favors the delocalization and accumulation of photogenerated holes, hence it can potentially catalyze dioxygen generation with four-electron transfer driven by visible light. In 2004, Kirner *et al.* reported that phosphonate-functionalized PDI-sensitized CoO_x as an effective photoelectrocatalyst to realize oxidation of H_2O, wherein PDI is not a photocatalyst[217]. Another similar work is from Finke's group in 2017[218]. Early in 2000, Linkous *et al.* first used a PDI derivative as the O_2-evolving photocatalyst when screening a series of prospective compounds[219]. The first systematical report using PDI self-assembly as a photocatalyst for water oxidation is Würthner's work in 2012[220]. They embedded Ru(Ⅱ) into the PDI nanofibers to enhance its performance. But Ru(Ⅱ) centers were assumed to be reaction sites, and the PDI aggregation mainly shielded the active Ru(Ⅱ) sites and decelerated their oxidation. In 2016, PTCDA nanorods were used by Wu's group as a photocatalytic oxidation system with an aid of CoO_x[221]. A major advance in this field came in 2016, when Zhu's group applied pure PDI self-assembled supramoleculars for the first time in an attempt to realize photolysis of water to generate dioxygen[64]. After that, a series of PDI self-assemblies with different side chains were developed to improve their photocatalytic dioxygen production performances[19, 74]. And then Kang *et al.* reported a Co-integrating PDI self-assembly for photocatalytic oxygen evolution with fast electron-hole separation (0.07 ps) and long recombination time (106.1 ps) between adjacent (011) and (002) side facets of Co-PDI aggregation[222]. The mechanism of photocatalytic dioxygen production over PDI self-assembly is as follows: (1) Under the excitation of visible light, the electrons in the VB of PDI self-assembly are excited to the CB to form photogenerated carriers; whereas the real separation of photogenerated charges is not realized, and the electrons in the CB would relax to the VB; (2) The Π–Π stacking structure in PDI self-assembly promotes the spatial separation of photogenerated electrons and holes via electron transfer, avoiding their recombination; (3) With the cumulative absorption of four photons by PDI self-assembly, the photogenerated electrons and holes are accumulated on the surface of PDI self-assembly and four-electron exchange with H_2O molecules occurs in the presence of electron sacrificial agents such as Ag^+ (Fig. 9(a)). In order to further transcend oxygen production performance of PDI self-assembly, the researchers also utilized some other suitable materials to combine with PDI self-assembly to construct better-performing composite photocatalysts, such as In_2O_3/PDI[223], Ag_2S/PDI[83], C_{60}/PDI[85] and Bi_2WO_6/PDI[208]. In addition, due to the electron-defective characteristics of PDI molecules, PDI molecules would exhibit an electron-transfer effect with the other linking motif such as $Cp^*Ir(ppy)Cl$ complex, making the linking part into strong high-valence oxidation states, which may accelerate the oxidation of water[224].

5.2.2. H_2 evolution

Generally, the potential of the CB of PDI self-assembly is lower than the reduction potential of H^+/H_2; therefore, the kinetic process of its photocatalytic dihydrogen production is unfavorable in thermodynamics. In terms of photocatalytic dihydrogen production, PDIs were initially considered as dye-sensitizers or co-catalysts to assist photocatalytic hydrolysis of host photocatalysts, mainly benefiting from its strong visible-light absorption, photochemical stability and energy level matching with $Zn_{0.5}Cd_{0.5}S$, TiO_2 or C_3N_4[87, 88, 225–227]. In order to make a breakthrough in photocatalytic dihydrogen evolution using PDI self-assembly, it needs to combine with other photocatalysts bearing dihydrogen production ability. Chen and coworkers succeeded in achieving the photocatalytic hydrogen production performance via constructing a C_3N_4/PDI composite catalyst for the enhanced performance, mainly because the photogenerated holes in C_3N_4 are assumed to rapidly transfer to the PDI moelcules, which effectively prevented the recombination of photogenerated electrons and holes in C_3N_4[87]. Sun *et al.* fabricated a PDI/$Zn_{0.5}Cd_{0.5}S$ composite with PDI as an electron collector for the inhibition of photogenerated charge recombination[226]. All these studies regarded PDI as a kind of auxiliary catalyst but not host photocatalysts. Importantly, the photocatalytic H_2 production function over PDI self-assembly can be achieved via appropriate modification to PDI molecules. In 2016, Li *et al.* revealed that PDI with incorporation with bipyridyl moieties into the network led to the enhancement of photocatalytic H_2 production performance[228]. In 2017, Nolan *et al.* found the photocatalytic H_2 production performance over PDI self-assembly can be modulated via fine-tuning of the pH of PDI assemblies[229]. In addition, with pyran embedded at the perylene ring of PDI molecules, Wang *et al.* achieved UV-driven producing H_2 process over PDI self-assembly[230]. Recently, Kong *et al.* modified side chains of PDI molecules with substituents phosphoric acid to achieve superior H_2 evolution performance with apparent quantum yield of

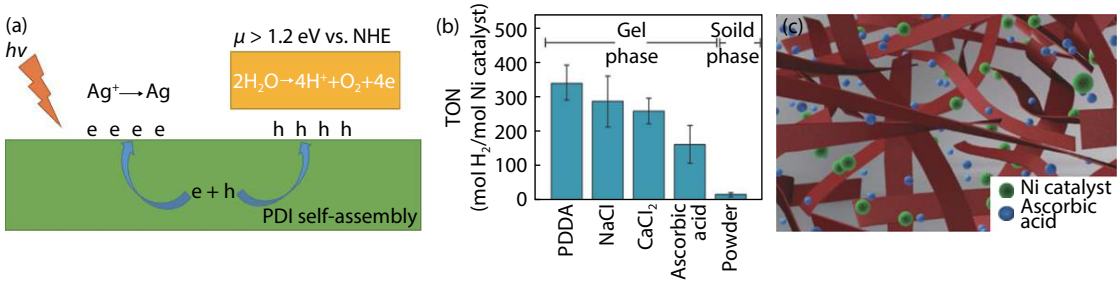

Fig. 9. (Color online) (a) The photocatalytic process with charge transfer and accumulation on the surface of PDI self-assembly. (b) H_2 production histogram of CA gels prepared with NaCl, PDDA, $CaCl_2$ and ascorbic acid compared to insoluble protonated CA with permission from Ref. [70]. All gel phases produce more H_2 than the solid-phase CA powder. (c) Schematic of gel showing that CA nanoribbons (in red) trap solvent water molecules (not shown for clarity) within a 3D architecture with permission from Ref. [70].

2.96% at 550 nm[231]. It is worth noting that PDI anion radicals in PDI self-assembly possess a strong reducing capability and hold great potential for photocatalytic H_2 production albeit a very small amount generated in PDI self-assembly[9]. Concomitantly, one of the conditions for photocatalytic H_2 production is photogenerated electron accumulation on the surface of PDI self-assembly. This determines that isolated PDI molecules, PDI anion radicals or PDI dianion radicals do not photocatalyze H_2 production except sufficient photoinduced multielectron/multiproton collection on the surface and appropriate reduction potentials[232]. In addition, excited PDI anion radicals can accelerate the transfer of photogenerated charges into host catalysts for further water splitting. Recently, Xu *et al.* achieved a highly efficient photocatalytic H_2 production with PDI anion radical sensitized TiO_2 as the photocatalyst. It was assumed that the consecutive charging of PDI driven by two-photon absorption steps enabled electron delivery from PDI anion radicals to TiO_2[233]. Moreover, the electron-ion interactions of PDI and TiO_2 were proposed by Li *et al.* to reveal charge transfer from PDI to TiO_2[234]. An example of using PDI self-assembly as a photocathode comes from Yao's work on photoelectrocatalytic dihydrogen production. The accumulation of photogenerated electrons in the PDI self-assembly led to its disaggregate, but this problem on stability was well-resolved by constructing the interface of the PDI self-assembly and RuO_2 because the electrons in the PDI self-assembly quickly migrated to RuO_2[235].

It is worth mentioning (perylene monoimide) PMI molecules whose structure is mostly similar to PDI molecules. Unlike the PDI scaffold, PMI molecules bear only one part of amide and side chain, but it can also form a supramolecular self-assembly by Π–Π stacking behaviors, and Π-electrons inside can migrate along the Π–Π stacking direction. The photocatalytic hydrogen production driven by hydrogel scaffold built with PMI supramolecular self-assembly was attempted by Stupp's group in 2014[70]. They found that by screening different catalysts and electrolytes to prepare the PMI self-assembled nanoribbons for 3D architecture, the electronic coupling interaction in the PMI self-assembly containing Ni catalyst can be changed, thereby triggering different photocatalytic properties (Figs. 9(b) and 9(c)). In 2015, they separated the hydrophobic core and hydrophilic carboxylate headgroup with the linkage of different alkyl lengths, and upon the addition of salt, a series of PMI self-assembled nanostructures were constructed[236]. It was inferred that due to exciton splitting efficiencies originated from their higher orbital overlap, these hydrogel self-assemblies exhibited productive photocatalytic dihydrogen amount. In 2017, they revealed that under the thermal driving, in a salt-containing solution, the transition of PMI self-assembly took place from a metastable state to a stable crystalline phase[237]. For the stable crystalline phase, a short scroll self-assembly formed at higher ionic strengths whereas long helical ribbons were generated at lower salt amount. Under irradiation, the stable PMI crystal phase generated charge-transfer excitons, which showcased enhanced photocatalytic dihydrogen production. Different substituents would affect the morphology and charge transport behavior in PMI self-assembly[238]. Molecular dipole strength affects the electronic coupling within PMI self-assembly, thereby changing its photocatalytic capability[239]. Electron-withdrawing substituents have a stronger molecular dipole strength to PMI, so its photocatalytic performance is superior to PMI self-assembly with electron-donating substituents. In addition, a three-dimensional hybrid hydrogel architecture consisting of –COOH-containing PMI self-assembly and polyelectrolyte (PE) gel was constructed to achieve improved photocatalytic H_2 production[240]. The opposite surface charges of PMI and PE improved the binding interaction of PMI assembly and PE gel and the mechanical characteristics of PMI self-assembly. The three-dimensional construction made it possible for the rapid in/out of substrates/products. Most recently, Stupp's group reviewed the relative contents on supramolecular energy materials[241].

5.3. Organic synthesis

In past decades, visible light-mediated organic synthesis has been derived as a very useful tool for building various natural products, medicine chemicals and organic functional materials[242]. The photocatalysts including homogeneous and heterogeneous systems provide sufficient power to drive redox reaction kinetics through photon absorption, charge separation and electron transfer. In general, unlike photocatalytic hydrolysis, the accumulation of photogenerated charges in photocatalytic organic synthesis is not necessary. Compared to traditional organic synthesis, heterogeneous photocatalytic organic synthesis has the following advantages: (1) The energy for driving the reaction could be from sustainable solar energy in line with the metrics of "green chemistry"[243]; (2) The redox agents are lots of small primary batteries inside excited photocatalysts, avoiding the use of expensive toxic reagents and improving its atom economy; (3) The heterogeneous photocatalysts could be recycled and reused via simple treat-

ment of removing surface chemical absorbates remaining.

Under visible-light excitation, PDI molecules would undergo direct single-electron transfer with some reducing agents to propagate some active intermediate species-PDI anion radicals with strong reducing ability. Accordingly, Ghosh *et al.* used PDI as a homogeneous photocatalyst to reduce a series of chlorinated compounds, achieving the effect of dehalogenation. After that, Schanze's group provided a direct evidence for the photoinduced electron-transfer process from excited PDI anion radicals to aromatic halogen via transient absorption spectra[244]. Visible-light photoredox catalysis initiated by radical anions has been reviewed by Ghosh[245]. Taking this as a reference, Zeng *et al.* fabricated a polymerized self-assembly through the coordination of Zn^{2+} and PDI with the side chains containing –COOH, which can catalyze organic reduction reactions such as dehalogenation and C–C bond coupling under visible-light irradiation. The ordered arrangement of the PDI self-assembly provided sufficient reaction sites for the reduction reactions and sufficient space for PDI to interact with the substrates, and decreased the self-quenching of PDI. As such, this heterogeneous photocatalyst demonstrated a better visible-light photocatalytic dehalogenation performance. Single crystal analysis revealed the polymer structure constructed by PDI and Zn^{2+}. They found that PDI absorbed a photon to form excited PDI firstly, which can oxidize triethylamine and then accept an electron of triethylamine to obtain PDI anion radicals. Importantly, the PDI anion radicals were excited again driven by visible light to yield highly reducing excited states. The coordination between PDI and Zn^{2+} and the Π–Π stacking structure between PDI molecules promoted the transfer of photogenerated charges, and stabilized the active sites of PDI anion radicals and catalyst-substrate interactions. Shang *et al.* also fabricated a heterogeneous photocatalyst for reducing aryl halides, but their method was covalently binding PDI on the surface of nanosilica[246]. Composites consisting of PDI and other materials are also deployed in synergistically photocatalytic organic synthesis. Poly(fluorine-PDI) arrays (PFPDI) were synthesized upon still reaction and then combined with graphene sheets[90]. The composite can catalyze the reduction of 4-nitrophenol to 4-aminophenol under visible-light irradiation attributable to the unique photophysical and redox properties.

However, the reducing capability of PDI self-assembly is rather weak, so it needs some extra driving conditions to achieve the effect of photocatalytic organic reduction. First, we can use some electron-donating chemicals (such as triethylamine or ammonia) to stabilize photo-generated electrons in PDI self-assembly and extend their lifetimes rest on the surface of PDI self-assembly; second, PDI generates a few PDI anion radicals in PDI self-assembly under the excitation of visible light. Upon re-excitation by light, PDI anion radicals absorb photons once again to form an excited state with stronger reducing power. DFT calculations showcase that the reduction potentials of PDI anion radicals and their excited states are –1.22 and +1.22 eV, respectively, which are much higher than the potentials of LUMO and HOMO levels of PDI molecules corresponding to –3.57 and –6.11 eV, respectively[8]. The reduction potential is sufficient to reduce a series of halogenated aromatic compounds.

There are still some difficulties that need to be resolved in photocatalytic organic synthesis over PDI self-assembly. For example, if PDI molecules are electronically coupled with metal ions, photogenerated electrons and active intermediate species may be quenched due to electron/energy transfer, which would in turn reduce photocatalytic efficacy of PDI self-assembly. Therefore, it is critical to select a suitable metal ion as a coupling agent with PDI. On the other hand, the aforementioned heterogeneous PDI self-assembly presents excellent photocatalytic efficiency, mainly because of Π–Π stacking structure. However, in real photocatalytic process, PDI self-assembly easily depolymerizes due to the change in the surrounding environment, which distorts the highly ordered Π–Π stacking structure.

5.4. Photodynamic/photothermal therapy

PDI self-assembly displays excellent photogenerated charge separation capability, generating photogenerated electrons and holes. Moreover, along the Π–Π stacking direction in PDI self-assembly, photogenerated electrons and holes can be separated spatially. Through energy/electron transfer, photogenerated electrons on the surface of PDI self-assembly would interact with O_2 to form singlet oxygen species ($^1O_2$) and superoxide radicals ($^{\bullet}O_2^-$), which play an important role in photocatalytic degradation. The holes in PDI self-assembly can oxidize organic pollutants and water molecules. Cancer is undoubtedly a huge threat to human physical health. Cancer treatment is a great challenge encountered in modern medical field. The currently used cancer treatment methods generally include surgical resection, chemotherapy, radiotherapy, endocrine therapy, and immunotherapy. But these traditional treatments may cause irreparable harm to the organizations. PDI self-assembly is a relatively safe and biocompatible chemical[77], and these generated active species could suppress or even remove tumor cells. Zhu's group investigated the photocatalytic anticancer effect through PDI self-assembly on skin tumor cells[19]. Two types of PDI self-assemblies with different stacking arrangements (H- and J-type) were prepared, respectively. The results proved that the J-type PDI self-assembly exhibited a higher inhibitory effect on cancer cell growth than the H-like counterpart due to intracellular singlet oxygen production (Figs. 10(a) and 10(b)). By regulating the Π–Π stacking structure, its photocatalytic anticancer effect can be enhanced due to light absorption at near-infrared region[77]. Another example using PDI self-assembly in the field of photocatalysis is the work of Chen's research group on antibacterial therapy[247]. Antibacterial therapy is a broad medical research field, and scientists have successfully connected photocatalysis with antibacterial therapy using inorganic semiconductors. Here they successfully distributed the PDI self-assembly on the surface of g-C_3N_4, obtaining PDI/g-C_3N_4 composite photocatalyst, and employed it for antibacterial treatment. The light absorption range of the composite photocatalyst was extended to 750 nm, and under irradiation, some active oxygen species, such as $^{\bullet}O_2^-$, $^1O_2$, $OH^{\bullet}$, were produced to suppress bacteria in vivo.

In addition, PDI-based organic semiconductors are widely used in photoacoustic imaging and photothermal therapy because of their thermal stability, high light-to-heat conversion, and simple modifiability[248–253]. Chen's group fabricated phototheranostic hollow mesoporous nanoparticles with hollow mesoporous organosilica (HMO) hybridized by

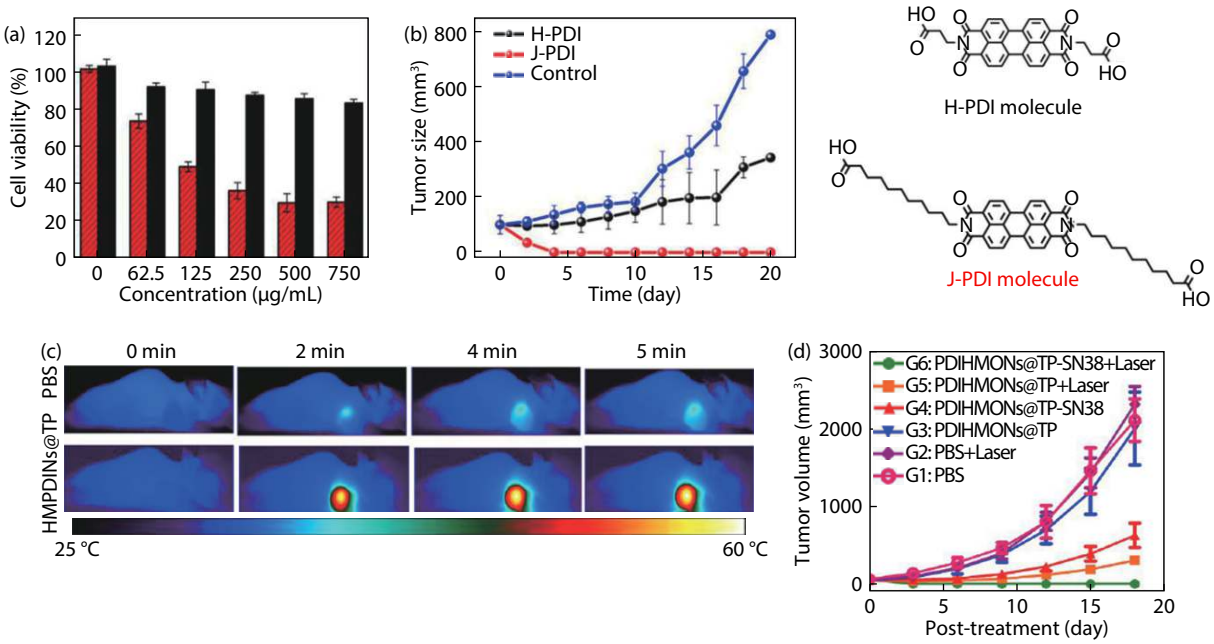

Fig. 10. (Color online) (a) In vitro viability of HeLa cells with different concentrations of H-PDI and J-PDI at 600 ± 15 nm with permission from Ref. [19]. (b) Time-dependent tumor growth in a murine tumor model after treated with H-PDI and J-PDI with permission from Ref. [19]. (c) Thermal images of U87MG tumor-bearing mice after treatment with PBS and HMPDINs@TP upon 671 nm laser irradiation with permission from Ref. [84]. (d) Tumor growth curves of the mice after different treatments with permission from Ref. [89].

PDI as a viable platform for controlled drug delivery/release and precise photoimaging[89]. The synergistic effect of PDI and HMO enhanced the fluorescence and photoacoustic signals to locate the target tumor region. Under the irradiation of near-infrared light, photothermal conversion showed up in the PDI self-assembly with an increase of temperature to 55 °C (Fig. 10(c)). The PDI self-assembly then disaggregated to control drug release targeted at tumor regions, leading to tumor ablation without recurrence treated with HMPDINs@TP-SN38 plus laser (Fig. 10(d)).

6. Summary and outlook

As a common pigment, the structure of the PDI molecule contains a large Π-conjugated perylene, cyclic amides and side chains. DFT calculations present that the C=C bond between the two naphthalene units of PDI molecule has the characteristics of the C–C bond, so that certain rotational distortion comes up. Unlike most of dyes, PDI molecules have one important feature, that is, through Π–Π stacking interaction and side-to-side chain effect, PDI molecules can aggregate to form supramolecular self-assembly with PDI molecules as building blocks. We can change PDI molecule structures by modification to perylene bay and side chains of PDI molecules. For one thing, the solubility of PDI molecules in organic solvents can thus be increased. On the other hand, the self-assembly mode of PDI molecules can be changed obviously, thereby effectively regulating morphology of PDI self-assembly. In a suitable solvent, the self-assembly process of PDI molecules occurs with controllable morphology through Π–Π stacking and side-to-side chain interactions. The PDI self-assembly methods include modifying PDI molecules with substituents, introducing metal ions, and changing dispersion solvents. The self-assembling of PDI molecules is a dynamic equilibrium process between aggregation and disaggregation, which is largely affected by PDI molecule structures and the external environment. According to this, the morphologies of PDI self-assembly can be effectively modulated to obtain desired well-defined supramolecular architectures. The PDI self-assembly has a band-like electronic structure with deep VB. In addition, the Π–Π stacking structure is conducive to the transfer of photogenerated charges along the Π–Π stacking direction, thereby reducing the recombination of photogenerated electrons and holes. Therefore, PDI self-assembly can be used in photocatalytic degradation, photocatalytic water splitting into H_2/O_2, photocatalytic organic synthesis and light-driven disease therapy. The emergency of the active species-PDI anion radicals in PDI self-assembly makes photocatalytic reduction possible in organic synthesis. A series of PDI self-assembly-based composites have been fabricated to further extend light absorption range, reduce recombination of photogenerated charges in PDI self-assembly, and increase the specific surface area of photocatalytic systems.

Whilst PDI self-assembly is a highly ordered supramolecular structure formed by PDI molecules through Π–Π stacking interaction, unlike C_3N_4, it is currently difficult to completely verify the clear structure of PDI self-assembly through theoretical calculations and experimental means, partly because non-covalent bonds make supramolecular structures some large variables[68]. Conventional characterization methods usually fail to determine the specific sequence of the internal structural units of the self-assembly, including not only the vertical aggregation of PDI molecules, but also the lateral interaction arrays. As one possible access, we can indirectly monitor the self-assembled process of PDI molecules to deduce the possible structure of PDI aggregates, in combination with structural analysis, which may require cross fusion of some in situ characterization techniques.

The overlapping of PDI molecular orbitals is beneficial to the formation of band-like electronic energy band structure.

Upon excitation by visible light, the electrons in the VB of PDI self-assembly transition to the conduction band, forming excited charge carriers. The charge carriers can move rapidly along the Π–Π stacking direction, thereby realizing the spatial separation of photogenerated electrons and holes. As an electron-defective pigment, neutral PDI molecules can be converted into PDI anion/dianion radicals, as well as existence in PDI self-assembly, but its real role in photocatalysis remains elusive except of photocatalytic organic synthesis, e.g. the reduction function of the excited states of anion/dianion radicals albeit the shorter lifetimes[182]. Now that PDI anion/dianion radicals are produced, PDI cation radical would also be generated, especially in highly ordered supramolecular[185]. The PDI cation radical may be very unstable so that photocatalytic oxidation process takes place smoothly. These active PDI intermediates may be unique in photocatalysis of PDI self-assembly, different from inorganic semiconductors.

In general, the electronic structure of PDI self-assembly can be further adjusted by modifying the electronic structure of the individual molecule. Since the Π–Π stacking interaction between PDI molecules has a significant effect on the electronic structure of PDI self-assembly, it is also a very effective way to modulate the PDI self-assembled mode. Such stacking arrangements are diversified, hence flexible electronic structure control can be achieved[78, 80]. In addition, due to the flexible supramolecular structure of PDI self-assembly, we can also construct PDI self-assembly with unique morphologies, such as three-dimensional porous/network structures with a large specific surface area, PDI self-assembly quantum dots, and multi-function photocatalytic materials coupling with other materials. However, the electronic energy band regulation of PDI self-assembly still faces some huge challenges as follows: first, the PDI self-assembled array is susceptible to interference from the external environment, and the regulation of the PDI self-assembled mode is unpredictable, which sometimes will cause a negative effect; secondly, PDI self-assembly may depolymerize due to the accumulation of photogenerated charges or the changed reaction conditions, thereby reducing its photocatalytic performance[198].

To further optimize the photocatalytic performance of the PDI self-assembly, we can proceed from three main aspects—enhancing the utilization of the full-spectrum sunlight, promoting the further separation of photogenerated charges, and building a stronger VB and CB potential. Though PDI self-assembly exhibits excellent visible light absorption performance, it lacks effective utilization of the ultraviolet region. This problem can be solved by modifying the molecular structures of PDI or combining with ultraviolet photocatalysts[10]. In general, the smaller the band gap, the greater the recombination probability of photogenerated electrons and holes, analogue to the energy gap law in large molecules[254], hence photogenerated charge recombination inside PDI self-assembly is also inevitable. To address the problem, we can construct an internal electric field in the molecules to leave the photogenerated electrons and holes to have a certain space, avoiding direct contact between them, or fabricate an n-p heterojunction to make the photogenerated electrons or holes conduct out timely. In order to leave the VB and CB potentials of the PDI self-assembly sufficient to drive the photocatalytic reaction, it is considerable to change PDI molecule structures or PDI stacking modes. In addition, the photocatalytic stability of PDI self-assembly also hinders its further development, and enhancing the interaction between PDI molecules inside is a feasible strategy that can be considered, such as connecting several PDI molecules in a series to increase the Π–Π stacking effect between PDI molecules, introducing polar functional groups or coordination bonds with metal ions to increase the side-to-side chain interactions.

Especially for the photocatalytic water splitting performance over PDI self-assembly, compared with other inorganic semiconductor materials, there is still a big gap in photocatalytic performance of PDI self-assembly. Under the interaction with water molecules, photo-generated charge conduction in PDI self-assembles may be hindered. On the other hand, the overpotentials of the photolytic water over PDI self-assembly are large, which is not conducive to the transport of photogenerated charges at the solid-liquid interface. To clarify the specific mechanism of the photocatalytic process is uncovering one of the keys of this door to explore the key factors that affect its photocatalytic performance. Using PDI self-assembly as a photocatalyst is a promising alternative to traditional photocatalysts. It can be believed that in the near future, this type of photocatalysts will make a greater breakthrough progress in photocatalysis and function as traditional photocatalysts.

Acknowledgements

We acknowledge the financial support from the National Natural Science Foundation of China (No. 21972052). We appreciate Prof. Yongfa Zhu from Tsinghua University for his suggestions to this review paper. S.O. thanks the financial support from the "Guizi Scholar" Program of Central China Normal University.

References

[1] Bard A J. Photoelectrochemistry. Science, 1980, 207, 139
[2] Hoffmann M R, Martin S T, Choi W, et al. Environmental applications of semiconductor photocatalysis. Chem Rev, 1995, 95, 69
[3] Quay P D, Tilbrook B, Wong C S. Oceanic uptake of fossil fuel CO_2: Carbon-13 evidence. Science, 1992, 256, 74
[4] Gustafsson O, Krusa M, Zencak Z, et al. Brown clouds over south asia: biomass or fossil fuel combustion. Science, 2009, 323, 495
[5] Wigley T M L. Could reducing fossil-fuel emissions cause global warming. Nature, 1991, 349, 503
[6] Tong H, Ouyang S, Bi Y P, et al. Nano-photocatalytic materials: Possibilities and challenges. Adv Mater, 2012, 24, 229
[7] Kudo A, Miseki Y. Heterogeneous photocatalyst materials for water splitting. Chem Soc Rev, 2009, 38, 253
[8] Wei W Q, Liu D, Wei Z, et al. Short-range π–π stacking assembly on P25 TiO_2 nanoparticles for enhanced visible-light photocatalysis. ACS Catal, 2017, 7, 652
[9] Wei W Q, Wei Z, Liu D, et al. Enhanced visible-light photocatalysis via back-electron transfer from palladium quantum dots to perylene diimide. Appl Catal B, 2018, 230, 49
[10] Wei W Q, Zhu Y F. TiO_2@perylene diimide full-spectrum photocatalysts via semi-core –shell structure. Small, 2019, 15, 1903933
[11] Hu W, Lin L, Zhang R Q, et al. Highly efficient photocatalytic water splitting over edge-modified phosphorene nanoribbons. J

Am Chem Soc, 2017, 139, 15429
[12] Fujito H, Kunioku H, Kato D, et al. Layered perovskite oxychloride Bi_4NbO_8Cl: A stable visible light responsive photocatalyst for water splitting. ChemInform, 2016, 138, 2082
[13] Wei Z, Liu M L, Zhang Z J, et al. Efficient visible-light-driven selective oxygen reduction to hydrogen peroxide by oxygen-enriched graphitic carbon nitride polymers. Energy Environ Sci, 2018, 11, 2581
[14] Zeng G T, Qiu J, Li Z, et al. CO_2 reduction to methanol on TiO_2-passivated GaP photocatalysts. ACS Catal, 2014, 4, 3512
[15] Li X, Yu J G, Jaroniec M, et al. Cocatalysts for selective photoreduction of CO_2 into solar fuels. Chem Rev, 2019, 119, 3962
[16] Zeng L, Liu T, He C, et al. Organized aggregation makes insoluble perylene diimide efficient for the reduction of aryl halides via consecutive visible light-induced electron-transfer processes. J Am Chem Soc, 2016, 138, 3958
[17] Ghosh I, Ghosh T, Bardagi J I, et al. Reduction of aryl halides by consecutive visible light-induced electron transfer processes. Science, 2014, 346, 725
[18] Robertson P K J, Robertson J M C, Bahnemann D W. Removal of microorganisms and their chemical metabolites from water using semiconductor photocatalysis. J Hazard Mater, 2012, 211/212, 161
[19] Wang J, Liu D, Zhu Y F, et al. Supramolecular packing dominant photocatalytic oxidation and anticancer performance of PDI. Appl Catal B, 2018, 231, 251
[20] Fujishima A, Honda K. Electrochemical photolysis of water at a semiconductor electrode. Nature, 1972, 238, 37
[21] Chai Z G, Zeng T T, Li Q, et al. Efficient visible light-driven splitting of alcohols into hydrogen and corresponding carbonyl compounds over a Ni-modified CdS photocatalyst. J Am Chem Soc, 2016, 138, 10128
[22] Hu J Q, Liu A L, Jin H L, et al. A versatile strategy for shish-kebab-like multi-heterostructured chalcogenides and enhanced photocatalytic hydrogen evolution. J Am Chem Soc, 2015, 137, 11004
[23] Song H, Meng X G, Wang S Y, et al. Direct and selective photocatalytic oxidation of CH_4 to oxygenates with O_2 on cocatalysts/ZnO at room temperature in water. J Am Chem Soc, 2019, 141, 20507
[24] He W W, Kim H K, Wamer W G, et al. Photogenerated charge carriers and reactive oxygen species in ZnO/Au hybrid nanostructures with enhanced photocatalytic and antibacterial activity. J Am Chem Soc, 2014, 136, 750
[25] Zhang K, Liu J L, Wang L Y, et al. Near-complete suppression of oxygen evolution for photoelectrochemical H_2O oxidative H_2O_2 synthesis. J Am Chem Soc, 2020, 142, 8641
[26] Yu Y Y, Ma K, Zhuang R, et al. Hydroxyl-mediated formation of highly dispersed SnO_2/TiO_2 heterojunction via pulsed chemical vapor deposition to enhance photocatalytic activity. Ind Eng Chem Res, 2019, 58, 14655
[27] Wang Y Y, Jiang W J, Luo W J, et al. Ultrathin nanosheets g-C_3N_4@Bi_2WO_6 core-shell structure via low temperature reassembled strategy to promote photocatalytic activity. Appl Catal B, 2018, 237, 633
[28] Yang J J, Chen D M, Zhu Y, et al. 3D –3D porous Bi_2WO_6/graphene hydrogel composite with excellent synergistic effect of adsorption-enrichment and photocatalytic degradation. Appl Catal B, 2017, 205, 228
[29] Iwase A, Yoshino S, Takayama T, et al. Water splitting and CO_2 reduction under visible light irradiation using Z-scheme systems consisting of metal sulfides, CoO_x-loaded $BiVO_4$, and a reduced graphene oxide electron mediator. J Am Chem Soc, 2016, 138, 10260
[30] Zou Z G, Ye J H, Sayama K, et al. Direct splitting of water under visible light irradiation with an oxide semiconductor photocatalyst. Nature, 2001, 414, 625
[31] Weng B, Qi M Y, Han C, et al. Photocorrosion inhibition of semiconductor-based photocatalysts: Basic principle, current development, and future perspective. ACS Catal, 2019, 9, 4642
[32] Ghosh S, Kouame N A, Ramos L, et al. Conducting polymer nanostructures for photocatalysis under visible light. Nat Mater, 2015, 14, 505
[33] Yang F X, Cheng S S, Zhang X T, et al. 2D organic materials for optoelectronic applications. Adv Mater, 2018, 30, 1702415
[34] Cao S W, Low J, Yu J G, et al. Polymeric photocatalysts based on graphitic carbon nitride. Adv Mater, 2015, 27, 2150
[35] Zhao N N, Yan L M, Zhao X Y, et al. Versatile types of organic/inorganic nanohybrids: From strategic design to biomedical applications. Chem Rev, 2019, 119, 1666
[36] Li L L, Chen Y, Zhu J J. Recent advances in electrochemiluminescence analysis. Anal Chem, 2017, 89, 358
[37] Choudhuri I, Bhauriyal P, Pathak B. Recent advances in graphene-like 2D materials for spintronics applications. Chem Mater, 2019, 31, 8260
[38] Niu W H, Yang Y. Graphitic carbon nitride for electrochemical energy conversion and storage. ACS Energy Lett, 2018, 3, 2796
[39] Meng Z, Stolz R M, Mendecki L, et al. Electrically-transduced chemical sensors based on two-dimensional nanomaterials. Chem Rev, 2019, 119, 478
[40] Ong W J, Tan L L, Ng Y H, et al. Graphitic carbon nitride (g-C_3N_4)-based photocatalysts for artificial photosynthesis and environmental remediation: Are we a step closer to achieving sustainability. Chem Rev, 2016, 116, 7159
[41] Wang Z H, Hu X, Liu Z Z, et al. Recent developments in polymeric carbon nitride-derived photocatalysts and electrocatalysts for nitrogen fixation. ACS Catal, 2019, 9, 10260
[42] Wang X C, Maeda K, Thomas A, et al. A metal-free polymeric photocatalyst for hydrogen production from water under visible light. Nat Mater, 2009, 8, 76
[43] Takeda H, Kamiyama H, Okamoto K, et al. Highly efficient and robust photocatalytic systems for CO_2 reduction consisting of a Cu(I) photosensitizer and Mn(I) catalysts. J Am Chem Soc, 2018, 140, 17241
[44] Higgins R F, Fatur S M, Shepard S G, et al. Uncovering the roles of oxygen in Cr(III) photoredox catalysis. J Am Chem Soc, 2016, 138, 5451
[45] Hong D C, Kawanishi T, Tsukakoshi Y, et al. Efficient photocatalytic CO_2 reduction by a Ni(II) complex having pyridine pendants through capturing a Mg^{2+} ion as a lewis-acid cocatalyst. J Am Chem Soc, 2019, 141, 20309
[46] Zhang D, Wu L Z, Zhou L, et al. Photocatalytic hydrogen production from hantzsch 1, 4-dihydropyridines by platinum(II) terpyridyl complexes in homogeneous solution. J Am Chem Soc, 2004, 126, 3440
[47] Fernández S, Franco F, Casadevall C, et al. A unified electro- and photocatalytic CO_2 to CO reduction mechanism with aminopyridine cobalt complexes. J Am Chem Soc, 2020, 142, 120
[48] Xu B, Troian-Gautier L, Dykstra R, et al. Photocatalyzed diastereoselective isomerization of cinnamyl chlorides to cyclopropanes. J Am Chem Soc, 2020, 142, 6206
[49] Elvington M, Brown J, Arachchige S M, et al. Photocatalytic hydrogen production from water employing a Ru, Rh, Ru molecular device for photoinitiated electron collection. J Am Chem Soc, 2007, 129, 10644
[50] Cheung P L, Kapper S C, Zeng T, et al. Improving photocatalysis for the reduction of CO_2 through non-covalent supramolecular

assembly. J Am Chem Soc, 2019, 141, 14961
[51] Rabe E J, Corp K L, Sobolewski A L, et al. Proton-coupled electron transfer from water to a model heptazine-based molecular photocatalyst. J Phys Chem Lett, 2018, 9, 6257
[52] Wang C, Xie Z G, de Krafft K E, et al. Doping metal–organic frameworks for water oxidation, carbon dioxide reduction, and organic photocatalysis. J Am Chem Soc, 2011, 133, 13445
[53] Yang X J, Liang T, Sun J X, et al. Template-directed synthesis of photocatalyst-encapsulating metal-organic frameworks with boosted photocatalytic activity. ACS Catal, 2019, 9, 7486
[54] Chambers M B, Wang X, Ellezam L, et al. Maximizing the photocatalytic activity of metal–organic frameworks with aminated-functionalized linkers: Substoichiometric effects in MIL-125-NH_2. J Am Chem Soc, 2017, 139, 8222
[55] Wei P F, Qi M Z, Wang Z P, et al. Benzoxazole-linked ultrastable covalent organic frameworks for photocatalysis. J Am Chem Soc, 2018, 140, 4623
[56] Wan Y, Wang L, Xu H, et al. A simple molecular design strategy for two-dimensional covalent organic framework capable of visible-light-driven water splitting. J Am Chem Soc, 2020, 149(9), 4508
[57] Luo Q Z, Bao L L, Wang D S, et al. Preparation and strongly enhanced visible light photocatalytic activity of TiO_2 nanoparticles modified by conjugated derivatives of polyisoprene. J Phys Chem C, 2012, 116, 25806
[58] Floresyona D, Goubard F, Aubert P H, et al. Highly active poly(3-hexylthiophene) nanostructures for photocatalysis under solar light. Appl Catal B, 2017, 209, 23
[59] Zhang M, Rouch W D, McCulla R D. Conjugated polymers as photoredox catalysts: Visible-light-driven reduction of aryl aldehydes by poly(p-phenylene). Eur J Org Chem, 2012, 2012, 6187
[60] Muktha B, Madras G, Guru Row T N, et al. Conjugated polymers for photocatalysis. J Phys Chem B, 2007, 111, 7994
[61] Ghosh S, Mallik A K, Basu R N. Enhanced photocatalytic activity and photoresponse of poly(3, 4-ethylenedioxythiophene) nanofibers decorated with gold nanoparticle under visible light. Sol Energy, 2018, 159, 548
[62] Li L W, Cai Z X, Wu Q H, et al. Rational design of porous conjugated polymers and roles of residual palladium for photocatalytic hydrogen production. J Am Chem Soc, 2016, 138, 7681
[63] Zhang Z J, Zhu Y F, Chen X J, et al. A full-spectrum metal-free porphyrin supramolecular photocatalyst for dual functions of highly efficient hydrogen and oxygen evolution. Adv Mater, 2019, 31, 1806626
[64] Liu D, Wang J, Bai X J, et al. Self-assembled PDINH supramolecular system for photocatalysis under visible light. Adv Mater, 2016, 28, 7284
[65] Wei Z, Hu J S, Zhu K J, et al. Self-assembled polymer phenylethnyl-copper nanowires for photoelectrochemical and photocatalytic performance under visible light. Appl Catal B, 2018, 226, 616
[66] Würthner F, Saha-Möller C R, Fimmel B, et al. Perylene bisimide dye assemblies as archetype functional supramolecular materials. Chem Rev, 2016, 116, 962
[67] Zollinger H. Color chemistry. 3rd ed. Wiley-VCH: Weinheim, 2003
[68] Wuerthner F. Perylene bisimide dyes as versatile building blocks for functional supramolecular architectures. ChemInform, 2004, 35, 1564
[69] Saito G, Yoshida Y. Development of conductive organic molecular assemblies: Organic metals, superconductors, and exotic functional materials. ChemInform, 2007, 38, 1
[70] Weingarten A S, Kazantsev R V, Palmer L C, et al. Self-assembling hydrogel scaffolds for photocatalytic hydrogen production. Nat Chem, 2014, 6, 964
[71] Ke D M, Zhan C L, Xu S P, et al. Self-assembled hollow nanospheres strongly enhance photoluminescence. J Am Chem Soc, 2011, 133, 11022
[72] Balakrishnan K, Datar A, Naddo T, et al. Effect of side-chain substituents on self-assembly of perylene diimide molecules: Morphology control. J Am Chem Soc, 2006, 128, 7390
[73] Bai S, Debnath S, Javid N, et al. Differential self-assembly and tunable emission of aromatic peptide bola-amphiphiles containing perylene bisimide in polar solvents including water. Langmuir, 2014, 30, 7576
[74] Wang J, Shi W, Liu D, et al. Supramolecular organic nanofibers with highly efficient and stable visible light photooxidation performance. Appl Catal B, 2017, 202, 289
[75] Balakrishnan K, Datar A, Oitker R, et al. Nanobelt self-assembly from an organic n-type semiconductor: Propoxyethyl-PTCDI. J Am Chem Soc, 2005, 127, 10496
[76] Jonkheijm P, van der Schoot P, Schenning A P H J, et al. Probing the solvent-assisted nucleation pathway in chemical self-assembly. Science, 2006, 313, 80
[77] Gong Q Y, Xing J, Huang Y J, et al. Perylene diimide oligomer nanoparticles with ultrahigh photothermal conversion efficiency for cancer theranostics. ACS Appl Bio Mater, 2020, 3, 1607
[78] Zang L. Interfacial donor–acceptor engineering of nanofiber materials to achieve photoconductivity and applications. Acc Chem Res, 2015, 48, 2705
[79] Che Y K, Datar A, Yang X M, et al. Enhancing one-dimensional charge transport through intermolecular π-electron delocalization: Conductivity improvement for organic nanobelts. J Am Chem Soc, 2007, 129, 6354
[80] Zang L, Che Y K, Moore J S. One-dimensional self-assembly of planar π-conjugated molecules: Adaptable building blocks for organic nanodevices. Acc Chem Res, 2008, 41, 1596
[81] Miao H, Yang J, Peng G L, et al. Enhancement of the degradation ability for organic pollutants via the synergistic effect of photoelectrocatalysis on a self-assembled perylene diimide (SA-PDI) thin film. Sci Bull, 2019, 64, 896
[82] Yang J, Miao H, Wei Y X, et al. Π-Π Interaction between self-assembled perylene diimide and 3D graphene for excellent visible-light photocatalytic activity. Appl Catal B, 2019, 240, 225
[83] Yang J, Miao H, Li W L, et al. Designed synthesis of a p-Ag_2S/n-PDI self-assembled supramolecular heterojunction for enhanced full-spectrum photocatalytic activity. J Mater Chem A, 2019, 7, 6482
[84] Miao H, Yang J, Wei Y X, et al. Visible-light photocatalysis of PDI nanowires enhanced by plasmonic effect of the gold nanoparticles. Appl Catal B, 2018, 239, 61
[85] Wei Y X, Ma M G, Li W L, et al. Enhanced photocatalytic activity of PTCDI-C60 via π-π interaction. Appl Catal B, 2018, 238, 302
[86] Zhang Z J, Wang J, Liu D, et al. Highly efficient organic photocatalyst with full visible light spectrum through π– π stacking of TCNQ–PTCDI. ACS Appl Mater Interfaces, 2016, 8, 30225
[87] Chen S, Wang C, Bunes B R, et al. Enhancement of visible-light-driven photocatalytic H_2 evolution from water over g-C_3N_4 through combination with perylene diimide aggregates. Appl Catal A, 2015, 498, 63
[88] Chen S, Jacobs D L, Xu J K, et al. 1D nanofiber composites of perylene diimides for visible-light-driven hydrogen evolution from water. RSC Adv, 2014, 4, 48486
[89] Yang Z, Fan W P, Zou J H, et al. Precision cancer theranostic platform by *in situ* polymerization in perylene diimide-hybridized hollow mesoporous organosilica nanoparticles. J Am Chem Soc, 2019, 141, 14687
[90] Stergiou A, Tagmatarchis N. Fluorene –perylene diimide arrays

onto graphene sheets for photocatalysis. ACS Appl Mater Interfaces, 2016, 8, 21576
[91] Chen S, Slattum P, Wang C Y, et al. Self-assembly of perylene imide molecules into 1D nanostructures: Methods, morphologies, and applications. Chem Rev, 2015, 115, 11967
[92] Huang C, Barlow S, Marder S R. Perylene-3, 4, 9, 10-tetracarboxylic acid diimides: Synthesis, physical properties, and use in organic electronics. J Org Chem, 2011, 76, 2386
[93] Peng H Q, Niu L Y, Chen Y Z, et al. Biological applications of supramolecular assemblies designed for excitation energy transfer. Chem Rev, 2015, 115, 7502
[94] Teo Y N, Kool E T. DNA-multichromophore systems. Chem Rev, 2012, 112, 4221
[95] Chen Z J, Debije M G, Debaerdemaeker T, et al. Tetrachloro-substituted perylene bisimide dyes as promising n-type organic semiconductors: Studies on structural, electrochemical and charge transport properties. ChemPhysChem, 2004, 5, 137
[96] Würthner F, Sautter A, Schilling J. Synthesis of diazadibenzoperylenes and characterization of their structural, optical, redox, and coordination properties. J Org Chem, 2002, 67, 3037
[97] Yan P, Chowdhury A, Holman M W, et al. Self-organized perylene diimide nanofibers. J Phys Chem B, 2005, 109, 724
[98] Che Y K, Datar A, Balakrishnan K, et al. Ultralong nanobelts self-assembled from an asymmetric perylene tetracarboxylic diimide. J Am Chem Soc, 2007, 129, 7234
[99] Che Y K, Huang H L, Xu M, et al. Interfacial engineering of organic nanofibril heterojunctions into highly photoconductive materials. J Am Chem Soc, 2011, 133, 1087
[100] Graser F, Hädicke E. Kristallstruktur und Farbe Bei Perylen-3, 4: 9, 10-bis(dicarboximid)-Pigmenten. Liebigs Ann Chem, 1980, 1980, 1994
[101] Graser F, Hädike E. Kristallstruktur und Farbe Bei Perylen-3, 4: 9, 10-bis(dicarboximid)-Pigmenten, 2. Liebigs Ann Chem, 1984, 1984, 483
[102] Struijk C W, Sieval A B, Dakhorst J E J, et al. Liquid crystalline perylene diimides: architecture and charge carrier mobilities. J Am Chem Soc, 2000, 122, 11057
[103] Datar A, Balakrishnan K, Yang X M, et al. Linearly polarized emission of an organic semiconductor nanobelt. J Phys Chem B, 2006, 110, 12327
[104] Yamagata H, Maxwell D S, Fan J, et al. HJ-aggregate behavior of crystalline 7, 8, 15, 16-tetraazaterrylene: Introducing a new design paradigm for organic materials. J Phys Chem C, 2014, 118, 28842
[105] Chen Y C, Lam J W Y, Kwok R T K, et al. Aggregation-induced emission: Fundamental understanding and future developments. Mater Horiz, 2019, 6, 428
[106] Che Y K, Yang X M, Liu G L, et al. Ultrathin n-type organic nanoribbons with high photoconductivity and application in optoelectronic vapor sensing of explosives. J Am Chem Soc, 2010, 132, 5743
[107] Rodler F, Schade B, Jäger C M, et al. Amphiphilic perylene–calix. J Am Chem Soc, 2015, 137, 3308
[108] Wang J L, Yu Y, Zhang L Z. Highly efficient photocatalytic removal of sodium pentachlorophenate with Bi_3O_4Br under visible light. Appl Catal B, 2013, 136/137, 112
[109] Liang Y M, Lan S Q, Deng P, et al. Regioregular and regioirregular poly(selenophene-perylene diimide) acceptors for polymer–polymer solar cells. ACS Appl Mater Interfaces, 2018, 10, 32397
[110] Li X, Wang H, Nakayama H, et al. Multi-sulfur-annulated fused perylene diimides for organic solar cells with low open-circuit voltage loss. ACS Appl Energy Mater, 2019, 2, 3805
[111] Samanta S K, Song I, Yoo J H, et al. Organic n-channel transistors based on. ACS Appl Mater Interfaces, 2018, 10, 32444
[112] Yang J, Yin Y, Chen F, et al. Comparison of three n-type copolymers based on benzodithiophene and naphthalene diimide/perylene diimide/fused perylene diimides for all-polymer solar cells application. ACS Appl Mater Interfaces, 2018, 10, 23263
[113] Woodhouse M, Perkins C L, Rawls M T, et al. Non-conjugated polymers for organic photovoltaics: Physical and optoelectronic properties of poly(perylene diimides). J Phys Chem C, 2010, 114, 6784
[114] Zhang J, Li Y, Huang J, et al. Ring-fusion of perylene diimide acceptor enabling efficient nonfullerene organic solar cells with a small voltage loss. J Am Chem Soc, 2017, 139, 16092
[115] An T C, An J B, Gao Y P, et al. Photocatalytic degradation and mineralization mechanism and toxicity assessment of antivirus drug acyclovir: Experimental and theoretical studies. Appl Catal B, 2015, 164, 279
[116] Iwase M, Yamada K, Kurisaki T, et al. Visible-light photocatalysis with phosphorus-doped titanium(IV) oxide particles prepared using a phosphide compound. Appl Catal B, 2013, 132/133, 39
[117] Kitano S, Hashimoto K, Kominami H. Photocatalytic degradation of 2-propanol over metal-ion-loaded titanium(IV) oxide under visible light irradiation: Effect of physical properties of nanocrystalline titanium(IV) oxide. Appl Catal B, 2011, 101, 206
[118] Li Q, Shang J K. Composite photocatalyst of nitrogen and fluorine codoped titanium oxide nanotube arrays with dispersed palladium oxide nanoparticles for enhanced visible light photocatalytic performance. Environ Sci Technol, 2010, 44, 3493
[119] Shi Q, Murcia-López S, Tang P Y, et al. Role of tungsten doping on the surface states in $BiVO_4$ photoanodes for water oxidation: Tuning the electron trapping process. ACS Catal, 2018, 8, 3331
[120] An L J, Onishi H. Electron–hole recombination controlled by metal doping sites in $NaTaO_3$ photocatalysts. ACS Catal, 2015, 5, 3196
[121] Liu X, Gao S, Xu H, et al. Stable blue TiO_{2-x} nanoparticles for efficient visible light photocatalysts. Nanoscale, 2013, 5, 1870
[122] Zhu Q, Peng Y, Lin L, et al. Green synthetic approach for Ti^{3+} self-doped TiO_{2-x} nanoparticles with efficient visible light photocatalytic activity. J Mater Chem A, 2014, 2, 4429
[123] Huang H W, Zhou C, Jiao X C, et al. Subsurface defect engineering in single-unit-cell Bi_2WO_6 monolayers boosts solar-driven photocatalytic performance. ACS Catal, 2020, 10, 1439
[124] Jiang D, Wang W Z, Zhang L, et al. Insights into the surface-defect dependence of photoreactivity over CeO_2 nanocrystals with well-defined crystal facets. ACS Catal, 2015, 5, 4851
[125] Cushing S K, Meng F K, Zhang J Y, et al. Effects of defects on photocatalytic activity of hydrogen-treated titanium oxide nanobelts. ACS Catal, 2017, 7, 1742
[126] Seybold G, Wagenblast G. New perylene and violanthrone dyestuffs for fluorescent collectors. Dye Pigment, 1989, 11, 303
[127] Sadrai M, Hadel L, Sauers R R, et al. Lasing action in a family of perylene derivatives: Singlet absorption and emission spectra, triplet absorption and oxygen quenching constants, and molecular mechanics and semiempirical molecular orbital calculations. J Phys Chem, 1992, 96, 7988
[128] Ahrens M J, Fuller M J, Wasielewski M R. Cyanated perylene-3, 4-dicarboximides and perylene-3, 4: 9, 10-bis(dicarboximide): Facile chromophoric oxidants for organic photonics and electronics. Chem Mater, 2003, 15, 2684
[129] Zhao Y Y, Wasielewski M R. 3, 4: 9, 10-Perylenebis(dicarboximide) chromophores that function as both electron donors and acceptors. Tetrahedron Lett, 1999, 40, 7047

[130] Lukas A S, Zhao Y Y, Miller S E, et al. Biomimetic electron transfer using low energy excited states: A green perylene-based analogue of chlorophylla. J Phys Chem B, 2002, 106, 1299
[131] Yoshida J I, Kataoka K, Horcajada R, et al. Modern strategies in electroorganic synthesis. Chem Rev, 2008, 108, 2265
[132] Kingston C, Palkowitz M D, Takahira Y, et al. A survival guide for the "electro-curious". Acc Chem Res, 2020, 53, 72
[133] Ruffoni A, Juliá F, Svejstrup T D, et al. Practical and regioselective amination of arenes using alkyl amines. Nat Chem, 2019, 11, 426
[134] Bariwal J, van der Eycken E. C–N bond forming cross-coupling reactions: An overview. Chem Soc Rev, 2013, 42, 9283
[135] Moeller K D. Synthetic applications of anodic electrochemistry. Tetrahedron, 2000, 56, 9527
[136] Yang Q L, Wang X Y, Lu J Y, et al. Copper-catalyzed electrochemical C–H amination of arenes with secondary amines. J Am Chem Soc, 2018, 140, 11487
[137] Morofuji T, Shimizu A, Yoshida J I. Electrochemical C–H amination: Synthesis of aromatic primary amines viaN-arylpyridinium ions. J Am Chem Soc, 2013, 135, 5000
[138] Ham W S, Hillenbrand J, Jacq J, et al. Divergent late-stage (hetero)aryl C–H amination by the pyridinium radical cation. Angew Chem Int Ed, 2019, 58, 532
[139] Hayashi R, Shimizu A, Yoshida J I. The stabilized cation pool method: Metal- and oxidant-free benzylic C–H/aromatic C–H cross-coupling. J Am Chem Soc, 2016, 138, 8400
[140] Hou Z W, Mao Z Y, Melcamu Y Y, et al. Back cover: Electrochemical synthesis of imidazo-fused N-heteroaromatic compounds through a C–N bond-forming radical. Angew Chem Int Ed, 2018, 57, 1722
[141] Hou Z W, Mao Z Y, Zhao H B, et al. Frontispiece: electrochemical C–H/N–H functionalization for the synthesis of highly functionalized (aza)indoles. Angew Chem Int Ed, 2016, 55, 9168
[142] Waldvogel S R, Selt M. Electrochemical allylic oxidation of olefins: Sustainable and safe. Angew Chem Int Ed, 2016, 55, 12578
[143] Jiang Y Y, Xu K, Zeng C C. Use of electrochemistry in the synthesis of heterocyclic structures. Chem Rev, 2018, 118, 4485
[144] Yan M, Kawamata Y, Baran P S. Synthetic organic electrochemical methods since 2000: On the verge of a renaissance. Chem Rev, 2017, 117, 13230
[145] Jutand A. Contribution of electrochemistry to organometallic catalysis. Chem Rev, 2008, 108, 2300
[146] Feng R Z, Smith J A, Moeller K D. Anodic cyclization reactions and the mechanistic strategies that enable optimization. Acc Chem Res, 2017, 50, 2346
[147] Krieg E, Weissman H, Shimoni E, et al. Understanding the effect of fluorocarbons in aqueous supramolecular polymerization: Ultrastrong noncovalent binding and cooperativity. J Am Chem Soc, 2014, 136, 9443
[148] Zhao Q L, Zhang S, Liu Y, et al. Tetraphenylethenyl-modified perylene bisimide: Aggregation-induced red emission, electrochemical properties and ordered microstructures. J Mater Chem, 2012, 22, 7387
[149] Hendsbee A D, Sun J P, Law W K, et al. Synthesis, self-assembly, and solar cell performance of N-annulated perylene diimide non-fullerene acceptors. Chem Mater, 2016, 28, 7098
[150] Li G, Zhao Y B, Li J B, et al. Synthesis, characterization, physical properties, and OLED application of single BN-fused perylene diimide. J Org Chem, 2015, 80, 196
[151] Seifert S, Schmidt D, Würthner F. An ambient stable core-substituted perylene bisimide dianion: Isolation and single crystal structure analysis. Chem Sci, 2015, 6, 1663
[152] Schuster N J, Joyce L A, Paley D W, et al. The structural origins of intense circular dichroism in a waggling helicene nanoribbon. J Am Chem Soc, 2020, 142, 7066
[153] Lee S K, Zu Y B, Herrmann A, et al. Electrochemistry, spectroscopy and electrogenerated chemiluminescence of perylene, terrylene, and quaterrylene diimides in aprotic solution. J Am Chem Soc, 1999, 121, 3513
[154] Zhang A D, Jiang W, Wang Z H. Fulvalene-embedded perylene diimide and its stable radical anion. Angew Chem, 2020, 132, 762
[155] Jones B A, Facchetti A, Wasielewski M R, et al. Tuning orbital energetics in arylene diimide semiconductors. materials design for ambient stability of n-type charge transport. J Am Chem Soc, 2007, 129, 15259
[156] Peurifoy S R, Castro E, Liu F, et al. Three-dimensional graphene nanostructures. J Am Chem Soc, 2018, 140, 9341
[157] Gao G P, Liang N N, Geng H, et al. Spiro-fused perylene diimide arrays. J Am Chem Soc, 2017, 139, 15914
[158] Liu B, Böckmann M, Jiang W, et al. Perylene diimide-embedded double. J Am Chem Soc, 2020, 142, 7092
[159] Langhals H. Cyclic carboxylic imide structures as structure elements of high stability. Novel developments in perylene dye chemistry. Heterocycles, 1995, 1, 477
[160] Wang W, Wang L Q, Palmer B J, et al. Cyclization and catenation directed by molecular self-assembly. J Am Chem Soc, 2006, 128, 11150
[161] Barendt T A, Ferreira L, Marques I, et al. Anion- and solvent-induced rotary dynamics and sensing in a perylene diimide. J Am Chem Soc, 2017, 139, 9026
[162] Pochas C M, Kistler K A, Yamagata H, et al. Contrasting photophysical properties of star-shaped vs linear perylene diimide complexes. J Am Chem Soc, 2013, 135, 3056
[163] Wang J, Yang Z, Gao X X, et al. Core-shell g-C_3N_4@ZnO composites as photoanodes with double synergistic effects for enhanced visible-light photoelectrocatalytic activities. Appl Catal B, 2017, 217, 169
[164] You C C, Würthner F. Self-assembly of ferrocene-functionalized perylene bisimide bridging ligands with Pt(II) corner to electrochemically active molecular squares. J Am Chem Soc, 2003, 125, 9716
[165] Delgado M C R, Kim E G, Filho D A D S, et al. Tuning the charge-transport parameters of perylene diimide single crystals via end and/or core functionalization: A density functional theory investigation. J Am Chem Soc, 2010, 132, 3375
[166] Kim Y J, Lee Y, Park K, et al. Hierarchical self-assembly of perylene diimide (PDI) crystals. J Phys Chem Lett, 2020, 11, 3934
[167] Zhou E J, Cong J Z, Wei Q S, et al. Berichtigung: all-polymer solar cells from perylene diimide based copolymers: Material design and phase separation control. Angew Chem, 2011, 123, 8120
[168] Luo Z H, Wu F, Zhang T, et al. Designing a perylene diimide/fullerene hybrid as effective electron transporting material in inverted perovskite solar cells with enhanced efficiency and stability. Angew Chem Int Ed, 2019, 58, 8520
[169] Dössel L F, Kamm V, Howard I A, et al. Synthesis and controlled self-assembly of covalently linked hexa-peri-hexabenzocoronene/perylene diimide dyads as models to study fundamental energy and electron transfer processes. J Am Chem Soc, 2012, 134, 5876
[170] Jin S B, Supur M, Addicoat M, et al. Creation of superheterojunction polymers via direct polycondensation: Segregated and bicontinuous donor–acceptor π-columnar arrays in covalent organic frameworks for long-lived charge separation. J Am Chem Soc, 2015, 137, 7817

[171] Prathapan S, Yang S I, Seth J, et al. Synthesis and excited-state photodynamics of perylene–porphyrin dyads. 1. parallel energy and charge transfer via a diphenylethyne linker. J Phys Chem B, 2001, 105, 8237
[172] O'Neil M P, Niemczyk M P, Svec W A, et al. Picosecond optical switching based on biphotonic excitation of an electron donor-acceptor-donor molecule. Science, 1992, 257, 63
[173] van der Boom T, Hayes R T, Zhao Y Y, et al. Charge transport in photofunctional nanoparticles self-assembled from zinc 5, 10, 15, 20-tetrakis(perylenediimide)porphyrin building blocks. J Am Chem Soc, 2002, 124, 9582
[174] Baram J, Shirman E, Ben-Shitrit N, et al. Control over self-assembly through reversible charging of the aromatic building blocks in photofunctional supramolecular fibers. J Am Chem Soc, 2008, 130, 14966
[175] Jung C, Müller B K, Lamb D C, et al. A new photostable terrylene diimide dye for applications in single molecule studies and membrane labeling. J Am Chem Soc, 2006, 128, 5283
[176] Marcon V, Breiby D W, Pisula W, et al. Understanding structure–mobility relations for perylene tetracarboxydiimide derivatives. J Am Chem Soc, 2009, 131, 11426
[177] Dsouza R N, Pischel U, Nau W M. Fluorescent dyes and their supramolecular host/guest complexes with macrocycles in aqueous solution. Chem Rev, 2011, 111, 7941
[178] Yin X M, Wang Q X, Zheng Y J, et al. Molecular alignment and electronic structure of N, N'-dibutyl-3, 4, 9, 10-perylene-tetracarboxylic-diimide molecules on MoS_2 surfaces. ACS Appl Mater Interfaces, 2017, 9, 5566
[179] Gigli L, Arletti R, Tabacchi G, et al. Structure and host-guest interactions of perylene-diimide dyes in zeolite L nanochannels. J Phys Chem C, 2018, 122, 3401
[180] Liu N, Shi M M, Pan X W, et al. Photoinduced electron transfer and enhancement of photoconductivity in silicon nanoparticles/perylene diimide composites in a polymer matrix. J Phys Chem C, 2008, 112, 15865
[181] Xie A F, Liu B, Hall J E, et al. Self-assembled photoactive polyelectrolyte/perylene-diimide composites. Langmuir, 2005, 21, 4149
[182] Gosztola D, Niemczyk M P, Svec W, et al. Excited doublet states of electrochemically generated aromatic imide and diimide radical anions. J Phys Chem A, 2000, 104, 6545
[183] Adegoke O O, Jung I H, Orr M, et al. Effect of acceptor strength on optical and electronic properties in conjugated polymers for solar applications. J Am Chem Soc, 2015, 137, 5759
[184] Shoaee S, Clarke T M, Huang C, et al. Acceptor energy level control of charge photogeneration in organic donor/acceptor blends. J Am Chem Soc, 2010, 132, 12919
[185] Dubey R K, Niemi M, Kaunisto K, et al. Direct evidence of significantly different chemical behavior and excited-state dynamics of 1, 7- and 1, 6-regioisomers of pyrrolidinyl-substituted perylene diimide. Chem Eur J, 2013, 19, 6791
[186] Ryan S T, Young R M, Henkelis J J , et al. Energy and electron transfer dynamics within a series of perylene diimide/cyclophane systems. J Am Chem Soc, 2015, 137, 15299
[187] Ramos A M, Beckers E H A, Offermans T, et al. Photoinduced multistep electron transfer in an oligoaniline –oligo(p-phenylene vinylene) –perylene diimide molecular array. J Phys Chem A, 2004, 108, 8201
[188] Ryan S T J, del Barrio J, Ghosh I, et al. Efficient host–guest energy transfer in polycationic cyclophane–perylene diimide complexes in water. J Am Chem Soc, 2014, 136, 9053
[189] Santos E R D, Pina J, Venâncio T, et al. Photoinduced energy and electron-transfer reactions by polypyridine ruthenium(II) complexes containing a derivatized perylene diimide. J Phys Chem C, 2016, 120, 22831
[190] Song Y, Zhang W, He S J, et al. Perylene diimide and luminol as potential-resolved electrochemiluminescence nanoprobes for dual targets immunoassay at low potential. ACS Appl Mater Interfaces, 2019, 11, 33676
[191] Huang Y W, Fu L N, Zou W J, et al. Ammonia sensory properties based on single-crystalline micro/nanostructures of perylene-diimide derivatives: Core-substituted effect. J Phys Chem C, 2011, 115, 10399
[192] Che Y K, Yang X M, Loser S, et al. Expedient vapor probing of organic amines using fluorescent nanofibers fabricated from an n-type organic semiconductor. Nano Lett, 2008, 8, 2219
[193] Schuster N J, Paley D W, Jockusch S, et al. Electron delocalization in perylene diimide helicenes. Angew Chem Int Ed, 2016, 55, 13519
[194] Ball M L, Zhang B Y, Xu Q Z, et al. Influence of molecular conformation on electron transport in giant, conjugated macrocycles. J Am Chem Soc, 2018, 140, 10135
[195] Malenfant P R L, Dimitrakopoulos C D, Gelorme J D, et al. N-type organic thin-film transistor with high field-effect mobility based on a N, N'-dialkyl-3, 4, 9, 10-perylene tetracarboxylic diimide derivative. Appl Phys Lett, 2002, 80, 2517
[196] Wang X Y, Meng J Q, Yang X, et al. Fabrication of a perylene tetracarboxylic diimide–graphitic carbon nitride heterojunction photocatalyst for efficient degradation of aqueous organic pollutants. ACS Appl Mater Interfaces, 2019, 11, 588
[197] Liu W Q, Bobbala S, Stern C L, et al. XCage: A tricyclic octacationic receptor for perylene diimide with picomolar affinity in water. J Am Chem Soc, 2020, 142, 3165
[198] Zhang Q C, Jiang L, Wang J, et al. Photocatalytic degradation of tetracycline antibiotics using three-dimensional network structure perylene diimide supramolecular organic photocatalyst under visible-light irradiation. Appl Catal B, 2020, 277, 119122
[199] Chen P, Blaney L, Cagnetta G, et al. Degradation of ofloxacin by perylene diimide supramolecular nanofiber sunlight-driven photocatalysis. Environ Sci Technol, 2019, 53, 1564
[200] Guldi D M. Fullerene–porphyrin architectures; photosynthetic antenna and reaction center models. Chem Soc Rev, 2002, 31, 22
[201] Liu L, Yue M T, Lu J R, et al. The enrichment of photo-catalysis via self-assembly perylenetetracarboxylic acid diimide polymer nanostructures incorporating TiO_2 nano-particles. Appl Surf Sci, 2018, 456, 645
[202] Araújo R F, Silva C J R, Paiva M C, et al. Efficient dispersion of multi-walled carbon nanotubes in aqueous solution by non-covalent interaction with perylene bisimides. RSC Adv, 2013, 3, 24535
[203] Liu Y, Zhu E W, Bian L Y, et al. Robust graphene dispersion with amphiphlic perylene-polyglycidol. Mater Lett, 2014, 118, 188
[204] Oelsner C, Schmidt C, Hauke F, et al. Interfacing strong electron acceptors with single wall carbon nanotubes. J Am Chem Soc, 2011, 133, 4580
[205] Tsarfati Y, Strauss V, Kuhri S, et al. Dispersing perylene diimide/SWCNT hybrids: Structural insights at the molecular level and fabricating advanced materials. J Am Chem Soc, 2015, 137, 7429
[206] Zhang K, Wang J, Jiang W J, et al. Self-assembled perylene diimide based supramolecular heterojunction with Bi_2WO_6 for efficient visible-light-driven photocatalysis. Appl Catal B, 2018, 232, 175
[207] Ji Q Y, Xu Z, Xiang W M, et al. Enhancing the performance of pollution degradation through secondary self-assembled composite supramolecular heterojunction photocatalyst BiOCl/PDI under visible light irradiation. Chemosphere, 2020, 253, 126751

[208] Gao Q Z, Xu J, Wang Z P, et al. Enhanced visible photocatalytic oxidation activity of perylene diimide/g-C_3N_4 n–n heterojunction via π–π interaction and interfacial charge separation. Appl Catal B, 2020, 271, 118933

[209] Wang H L, Zhao L L, Liu X Q, et al. Novel hydrogen bonding composite based on copper phthalocyanine/perylene diimide derivatives p–n heterojunction with improved photocatalytic activity. Dye Pigment, 2017, 137, 322

[210] Zeng W G, Cai T, Liu Y T, et al. An artificial organic-inorganic Z-scheme photocatalyst WO_3@Cu@PDI supramolecular with excellent visible light absorption and photocatalytic activity. Chem Eng J, 2020, 381, 122691

[211] Cheng Y, Song R Q, Wu K, et al. The enhanced visible-light-driven antibacterial performances of PTCDI-PANI(Fe(III)-doped) heterostructure. J Hazard Mater, 2020, 383, 121166

[212] Gao X M, Gao K L, Li X B, et al. Hybrid PDI/BiOCl heterojunction with enhanced interfacial charge transfer for a full-spectrum photocatalytic degradation of pollutants. Catal Sci Technol, 2020, 10, 372

[213] Jeon T H, Koo M S, Kim H, et al. Dual-functional photocatalytic and photoelectrocatalytic systems for energy- and resource-recovering water treatment. ACS Catal, 2018, 8, 11542

[214] Ding C M, Shi J Y, Wang Z L, et al. Photoelectrocatalytic water splitting: Significance of cocatalysts, electrolyte, and interfaces. ACS Catal, 2017, 7, 675

[215] Brereton K R, Bonn A G, Miller A J M. Molecular photoelectrocatalysts for light-driven hydrogen production. ACS Energy Lett, 2018, 3, 1128

[216] Sheng Y Q, Miao H, Jing J F, et al. Perylene diimide anchored graphene 3D structure via π–π interaction for enhanced photoelectrochemical degradation performances. Appl Catal B, 2020, 272, 118897

[217] Kirner J T, Stracke J J, Gregg B A, et al. Visible-light-assisted photoelectrochemical water oxidation by thin films of a phosphonate-functionalized perylene diimide plus CoO_x cocatalyst. ACS Appl Mater Interfaces, 2014, 6, 13367

[218] Kirner J T, Finke R G. Sensitization of nanocrystalline metal oxides with a phosphonate-functionalized perylene diimide for photoelectrochemical water oxidation with a CoO_x catalyst. ACS Appl Mater Interfaces, 2017, 9, 27625

[219] Linkous C A, Slattery D K. Solar photocatalytic hydrogen production from water using a dual bed photosystem-phase I final report and phase II proposal. Office of Scientific and Technical Information (OSTI), 2000

[220] Kunz V, Stepanenko V, Würthner F. Embedding of a ruthenium(ii) water oxidation catalyst into nanofibers via self-assembly. Chem Commun, 2015, 51, 290

[221] Li J X, Li Z J, Ye C, et al. Visible light-induced photochemical oxygen evolution from water by 3, 4, 9, 10-perylenetetracarboxylic dianhydride nanorods as an n-type organic semiconductor. Catal Sci Technol, 2016, 6, 672

[222] Zhong Z, Li R F, Lin W L, et al. One-dimensional nanocrystals of cobalt perylene diimide polymer with *in situ* generated FeOOH for efficient photocatalytic water oxidation. Appl Catal B, 2020, 260, 118135

[223] Zheng R J, Zhang M, Sun X, et al. Perylene-3, 4, 9, 10-tetracarboxylic acid accelerated light-driven water oxidation on ultrathin indium oxide porous sheets. Appl Catal B, 2019, 254, 667

[224] Vagnini M T, Smeigh A L, Blakemore J D, et al. Ultrafast photodriven intramolecular electron transfer from an iridium-based water-oxidation catalyst to perylene diimide derivatives. PNAS, 2012, 109, 15651

[225] Chen S, Li Y X, Wang C Y. Visible-light-driven photocatalytic H_2 evolution from aqueous suspensions of perylene diimide dye-sensitized Pt/TiO_2 catalysts. RSC Adv, 2015, 5, 15880

[226] Sun T, Song J G, Jia J, et al. Real roles of perylenetetracarboxylic diimide for enhancing photocatalytic H_2-production. Nano Energy, 2016, 26, 83

[227] Chen Y Z, Li A X, Yue X Q, et al. Facile fabrication of organic/inorganic nanotube heterojunction arrays for enhanced photoelectrochemical water splitting. Nanoscale, 2016, 8, 13228

[228] Li L W, Cai Z X. Structure control and photocatalytic performance of porous conjugated polymers based on perylene diimide. Polym Chem, 2016, 7, 4937

[229] Nolan M C, Walsh J J, Mears L L E, et al. pH dependent photocatalytic hydrogen evolution by self-assembled perylene bisimides. J Mater Chem A, 2017, 5, 7555

[230] Wang R, Li G, Zhang A D, et al. Efficient energy-level modification of novel pyran-annulated perylene diimides for photocatalytic water splitting. Chem Commun, 2017, 53, 6918

[231] Kong K Y, Zhang S C, Chu Y M, et al. A self-assembled perylene diimide nanobelt for efficient visible-light-driven photocatalytic H_2 evolution. Chem Commun, 2019, 55, 8090

[232] Concepcion J J, House R L, Papanikolas J M, et al. Chemical approaches to artificial photosynthesis. PANS, 2012, 109, 15560

[233] Xu Y C, Zheng J X, Lindner J O, et al. Consecutive charging of a perylene bisimide dye by multistep low-energy solar-light-induced electron transfer towards H_2 evolution. Angew Chem Int Ed, 2020, 59, 10363

[234] Li X, Lv X, Zhang Q Q, et al. Self-assembled supramolecular system PDINH on TiO_2 surface enhances hydrogen production. J Colloid Interface Sci, 2018, 525, 136

[235] Yao L, Guijarro N, Boudoire F, et al. Establishing stability in organic semiconductor photocathodes for solar hydrogen production. J Am Chem Soc, 2020, 142, 7795

[236] Weingarten A S, Kazantsev R V, Palmer L C, et al. Supramolecular packing controls H_2 photocatalysis in chromophore amphiphile hydrogels. J Am Chem Soc, 2015, 137, 15241

[237] Kazantsev R V, Dannenhoffer A J, Weingarten A S, et al. Crystal-phase transitions and photocatalysis in supramolecular scaffolds. J Am Chem Soc, 2017, 139, 6120

[238] Kazantsev R V, Dannenhoffer A J, Aytun T, et al. Molecular control of internal crystallization and photocatalytic function in supramolecular nanostructures. Chem, 2018, 4, 1596

[239] Weingarten A S, Dannenhoffer A J, Kazantsev R V, et al. Chromophore dipole directs morphology and photocatalytic hydrogen generation. J Am Chem Soc, 2018, 140, 4965

[240] Sai H, Erbas A, Dannenhoffer A, et al. Chromophore amphiphile-polyelectrolyte hybrid hydrogels for photocatalytic hydrogen production. J Mater Chem A, 2020, 8, 158

[241] Dumele O, Chen J H, Passarelli J V, et al. Supramolecular energy materials. Adv Mater, 2020, 32, 1907247

[242] Prier C K, Rankic D A, MacMillan D W C. Visible light photoredox catalysis with transition metal complexes: Applications in organic synthesis. Chem Rev, 2013, 113, 5322

[243] Anastas P T, Warner J. Green chemistry: Theory and practice. Oxford Univ Press, 1998

[244] Zeman C J IV, Kim S, Zhang F, et al. Direct observation of the reduction of aryl halides by a photoexcited perylene diimide radical anion. J Am Chem Soc, 2020, 142, 2204

[245] Ghosh I. Excited radical anions and excited anions in visible light photoredox catalysis. Phys Sci Rev, 2019, 4, 20170185

[246] Shang J T, Tang H Y, Ji H W, et al. Synthesis, characterization, and activity of a covalently anchored heterogeneous perylene diimide photocatalyst. Chin J Catal, 2017, 38, 2094

[247] Wang L W, Zhang X, Yu X, et al. An all-organic semiconductor

C_3N_4/PDINH heterostructure with advanced antibacterial photocatalytic therapy activity. Adv Mater, 2019, 31, 1901965

[248] Yang Z, Chen X Y. Semiconducting perylene diimide nanostructure: Multifunctional phototheranostic nanoplatform. Acc Chem Res, 2019, 52, 1245

[249] Hu X M, Lu F, Chen L, et al. Perylene diimide-grafted polymeric nanoparticles chelated with Gd^{3+} for photoacoustic/T1-weighted magnetic resonance imaging-guided photothermal therapy. ACS Appl Mater Interfaces, 2017, 9, 30458

[250] Tang W, Yang Z, Wang S, et al. Organic semiconducting photoacoustic nanodroplets for laser-activatable ultrasound imaging and combinational cancer therapy. ACS Nano, 2018, 12, 2610

[251] Yang Z, Tian R, Wu J J, et al. Impact of semiconducting perylene diimide nanoparticle size on lymph node mapping and cancer imaging. ACS Nano, 2017, 11, 4247

[252] Fan Q L, Cheng K, Yang Z, et al. Photoacoustic imaging: Perylene-diimide-based nanoparticles as highly efficient photoacoustic agents for deep brain tumor imaging in living mice. Adv Mater, 2015, 27, 774

[253] Lü B, Chen Y F, Li P Y, et al. Stable radical anions generated from a porous perylenediimide metal-organic framework for boosting near-infrared photothermal conversion. Nat Commun, 2019, 10, 767

[254] Englman R, Jortner J. The energy gap law for radiationless transitions in large molecules. Mol Phys, 1970, 18, 145